Article

Land Cover Changes and Driving Factors in the Source Regions of the Yangtze and Yellow Rivers over the Past 40 Years

Xiuyan Zhang [1,2], Yuhui Yang [1,2], Haoyue Gao [2,3], Shu Xu [2], Jianming Feng [2,4] and Tianling Qin [2,*]

1   College of Resource Environment and Tourism, Capital Normal University, Beijing 100048, China
2   State Key Laboratory of Simulation and Regulation of Water Cycle in River Basin, China Institute of Water Resources and Hydropower Research, Beijing 100038, China
3   School of Water Conservancy and Hydroelectric Power, Hebei University of Engineering, Handan 056038, China
4   School of Water Conservancy and Transportation, Zhengzhou University, Zhengzhou 450001, China
*   Correspondence: qintl@iwhr.com; Tel.: +86-151-1020-7834

Abstract: As a climate-sensitive region of the Tibetan Plateau, the source regions of the Yangtze and Yellow Rivers (SRYYRs) urgently require an analysis of land cover change (LUCCs) over a long period, high temporal resolution, and high spatial resolution. This study utilizes nearly 40 years of land cover, the Normalized Difference Vegetation Index (NDVI), climate, and geomorphological data, applying methods including a land transfer matrix, slope trend analysis, correlation analysis, and landscape pattern indices to analyze the spatial and temporal changes, composition, layout, and quality of the local land cover and the factors. The findings reveal that (1) the land cover area change rate was 8.96% over the past 40 years, the unutilized land area decreased by 24.49%, and the grassland area increased by 6.37%. The changes were obvious at the junction of the two source regions and the southeast side of the source region of the Yellow River. (2) the landscape pattern was more centralized and diversified. The number of low-cover grassland patches increased by 12.92%. (3) The region is still dominated by medium- and low-cover vegetation, with the mean annual NDVI increasing at a rate of 0.006/10a, and the rate of change after 2000 is three times higher than previously. (4) The degree of land cover change is greater in the middle altitudes, semisunny aspects, steepest slopes, and middle-relief mountains. Additionally, 76.8% of the region's vegetation growth is dominated by mean annual temperatures. This study provides fundamental data and theory for understanding LUCCs and the driving factors in alpine plateau regions.

Keywords: the source regions of the Yangtze and Yellow Rivers; spatial–temporal change in land cover; vegetation cover

1. Introduction

Global climate change significantly impacts natural ecosystems, such as vegetation communities and biodiversity [1]. This is especially evident in the Qinghai–Tibetan Plateau (TP) region, where the community structure is simple and ecosystems are fragile in terms of resistance to disturbance and self-repair [2]. The TP has long been considered a key region in influencing global climate change. With the acceleration of the warming and humidification process, glaciers on the TP and its surrounding areas have melted by nearly 1232.8 km^2 within the last 40 years, and climate change is surpassing other regions of the world [3–8]. Significant vegetation greening has occurred, and serious issues such as alpine grassland degradation and sandy wind have severely affected the regional ecosystem's carbon cycle and storage [9–14]. The source regions of the Yangtze and Yellow Rivers (SRYYRs), as the birthplace of these rivers, are crucial for grassland animal husbandry and alpine biodiversity. The glaciers, snow cover, frozen soil, and alpine grasslands in these regions provide stable ecological services to surrounding and downstream areas [15,16]. The area of frozen soil in the source regions of the Yellow River is decreasing at a rate of 1.1%

year by year, and the annual precipitation broke the historical record in 2018 [12,17–19]. The area of the permafrost region declined from 113,580 km^2 to 108,940 km^2 from 1981 to 2015, and its glacier mass loss was -0.343 ± 0.055 Gt yr^{-1} up to 2018, with an increase in the mean value of the thickness of the active layer [17,20–22]. An increasing amount of data suggest that the region faces a severe ecological challenge.

The land cover constitution is a visual expression of the dynamics of the terrestrial surface system, and understanding the long-term changes in the land cover and potential drivers in SRYYRs has become a pivotal link to promote the recovery of vegetation ecosystems within the regions in the TP, and even globally [23,24]. Under the combined influence of the Indian summer winds and the midlatitude westerly wind belt, there are regional differences in the distribution of vegetation and land use values in this region [25–27].

As an important bridge to connect soil, the atmosphere, and water in terrestrial ecosystems, many studies have focused on the coordinated relationship between climatic factors and vegetation growth, quantitatively describing the vegetation cover, growth conditions, and influencing factors in the region through trend analysis, correlation analysis, and geographical detectors [28–33]. Research indicates that in recent years, the strengthening of ecological protection means has promoted the continuous improvement in land cover change (LUCCs) in the source regions of the Yangtze and Yellow Rivers [26,32,34]. Over the past 20 years, the area and coverage of vegetation cover in the region have shown different degrees of increase due to ecological projects, while studies have shown that vegetation growth in the region is more temperature-dependent than precipitation-dependent [31,32,35–37].

Remote sensing data are the key data to quantify land cover and vegetation dynamics, and the Normalized Difference Vegetation Index, which can reflect the vegetation dynamics over a long time series, is the primary type of indicator [38,39]. However, different remote sensing datasets have their drawbacks; for example, the commonly used MODIS data can only show the vegetation changes in the last 20 years, and the GIMMS NDVI3g data, which have a longer time series, have a low spatial resolution [40]. The complex topography of the source region of the Yangtze and Yellow Rivers makes it difficult to characterize the trend in vegetation microvariation with a large-scale resolution, and it is difficult to measure the effectiveness of ecological protection means with a shorter temporal resolution.

Based on this, this paper analyzes the changes in land cover types in the SRYYRs. It discusses the changes in land cover and climatic factors under different topography and geomorphology factors by using land cover data from 1980 to 2020. Additionally, a multisource medium-resolution vegetation cover index dataset is constructed to explore the regions' vegetation growth quality and to improve the spatial resolution of remote sensing data for vegetation monitoring. By comparing the Yangtze and Yellow River source regions, this study intends to reveal the trend in the LUCCs and the climate-influencing factors in the source regions of the Yangtze and Yellow Rivers to provide references and lessons for sustainable development and the effectiveness of ecological protection measures.

2. Materials and Methods

2.1. Study Area

The source regions of the Yangtze and Yellow Rivers are situated between 90°55′ E~103°41′ E and 32°16′ N~36°12′ N, an area of about 26.44×10^4 km^2 (Figure 1), with an elevation ranging from 2665 m to 6575 m and dominated by the Qinghai–Nanjiang–Qiangtang grassland and desert, which is a semihumid–semiarid cold plateau ecosystem. The basic climate type is cold, alpine, and arid [41]. The source region of the Yangtze River serves as the most concentrated area for the distribution of the SRYYRs' glaciers, characterized by its towering terrain and consistently cold and dry climate throughout the year. The average altitude of the source regions of the Yellow River is lower than the source region of the Yangtze River, and the terrain is high in the west to low in the north, separated from the Jinsha River by the Bayan-Ka-La mountain range in the west and the Animachin Mountains in the north. The river meanders in the basin. There are diverse land cover types such as

grasslands, woodlands, and cultivated land, with grasslands being the most significant natural resource and ecological carrier. The dominant vegetation type is meadows [42].
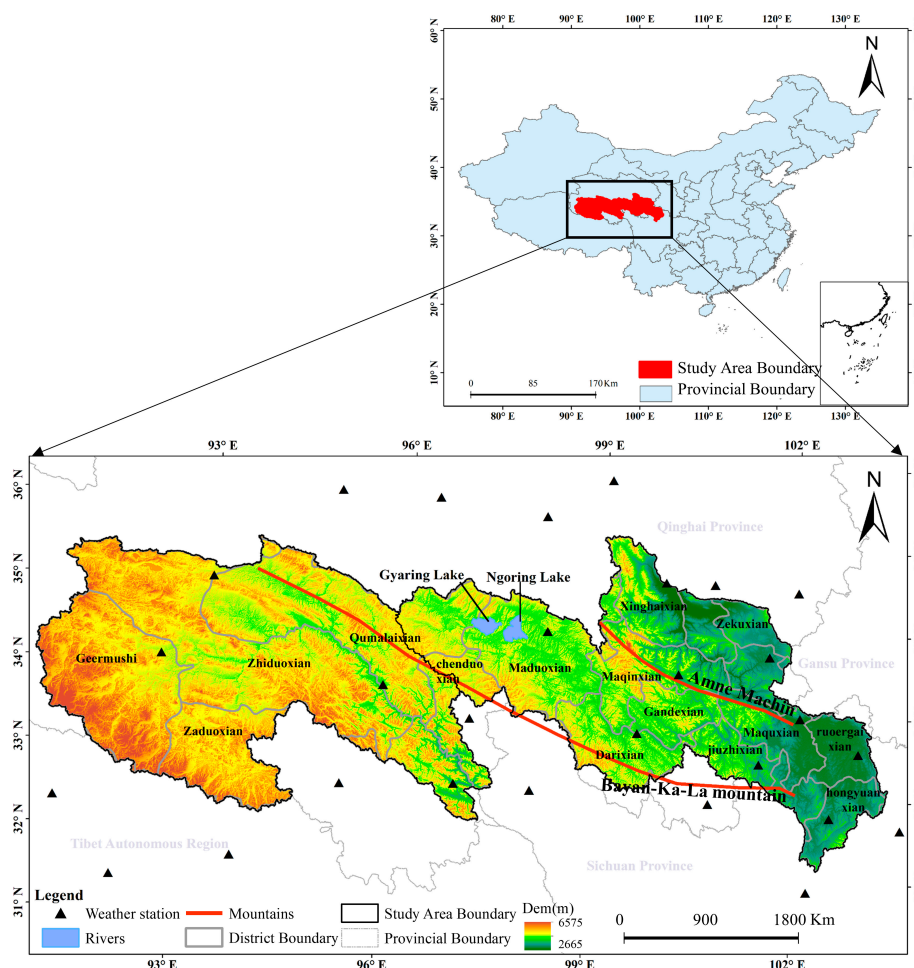
Figure 1. The location of hydrological and meteorological stations, river and lake, and altitude in and around the source regions of the Yangtze and Yellow Rivers. The study area is situated in the source region of the Yangtze River to its left and the source region of the Yellow River to its right.

2.2. Data Resources and Processing

2.2.1. Vegetation Data and Preprocessing

The Normalized Vegetation Index (NDVI) is the most widely utilized metric for monitoring vegetation growth. This study employed two vegetation index products: GIMMS NDVI3g and MOD13Q1 NDVI. The specific sources' spatial and temporal resolutions of these products are detailed in Table 1. Monthly values were derived by using the Monthly Maximum Value Synthesis (MVC) method, with the monthly average serving as the mean annual NDVI value for the study area. This approach was chosen to minimize the impact of extreme monthly values. Values of 0.1 or above were considered indicative of vegetation coverage. The mean annual NDVI data with a spatial resolution of 250 m for 1982–2020 were collected.

According to the existing literature, integrating GIMMS and MODIS data has been demonstrated to be effective in analyzing vegetation dynamics in the northern hemisphere [31,43]. The present study used the Temporal Adaptive Reflectance Fusion Model (ESTARFM) algorithm to calculate the mean annual NDVI data at a 250 m resolution from 1982 to 1999. This algorithm utilizes transformation coefficients to transform mixed pixel reflectance from coarse resolution to its constituent fine-resolution pixels. This approach

ensures precise reflectance estimations for small and linear features while maintaining spatial intricacies. The calculation formula is as follows:

$$F(x_w/2, y_{w/2}, t_p, B) = F(x_{w/2}, y_{w/2}, t_0, B) + \sum_{i=1}^{N} W_i \times V_i \times \left(C(x_i, y_i, t_p, B) - C(x_i, y_i, t_0, B) \right) \tag{1}$$

$$T_k = \frac{1/\left| \sum_{j=1}^{w} \sum_{i=1}^{w} C(x_i, y_j, t_k, B) - \sum_{j=1}^{w} \sum_{i=1}^{w} C(x_i, y_j, t_p, B) \right|}{\sum_{k=m,n} \left(1/\left| \sum_{j=1}^{w} \sum_{i=1}^{w} C(x_i, y_j, t_k, B) - \sum_{j=1}^{w} \sum_{i=1}^{w} C(x_i, y_j, t_p, B) \right| \right)} \quad k = (m, n) \tag{2}$$

where F and C denote the fine-resolution reflectance and coarse-resolution reflectance, respectively. (x_i, y_i) is the position of the i-th similar pixels; w is the size of the sliding window; W_i is the weight value of similar pixels to the central pixels, whereby the value range is 0–1; $(x_{w/2}, y_{w/2})$ is the center position of the pixels to be measured; (x_i, y_i) is the position of the i-th similar pixels; t_p, t_k, t_0 are the image-acquisition times; B is the image band; N is the number of similar pixels; V_i is conversion factor; and T_k is the reflectance of the central pixel:

$$W_i = (1/D_i) / \sum_{i=1}^{N} (1/D_i) \tag{3}$$

$$D_i = (1 - R_i) \times d_i \tag{4}$$

$$d_i = 1 + \sqrt{(x_{w/2} - x_i)^2 + (y_{w/2} - y_i)^2} / (w/2) \tag{5}$$

where w is the width of the searching window that is used to normalize the distance, ensuring that the distance range for similar pixels in different search windows extends from 1 to $1 + 2^{0.5}$. d_i is the geographic distance between the i-th similar pixel and central pixel; D_i is the product of the spectral similarity and spatial distance calculation of the central pixels and similar pixels; and R_i is the spectral similarity weight value, whereby the value range is −1–1.

Table 1. Sources of the fundamental data used.

Dataset	Data Sources	Time and Spatial Scale	
GIMMS NDVI3g	https://www.nasa.gov/ (accessed on 1 January 2023)	15 d 8 km	1982–2015
MOD13Q1 NDVI	http://e4ftl01.cr.usgs.gov (accessed on 1 January 2023)	16 d 250 m	2000–2020

By selecting two pairs of base data from corresponding time periods, the fine-resolution reflectance at t_p can be predicted based on the fine-resolution reflectance at the base date and the resampled coarse-resolution reflectance observed at t_p. Then, the final predicted fine-resolution reflectance at the prediction time t_p is calculated as [44]

$$F(x_{w/2}, y_{w/2}, t_p, B) = T_m \times F_m(x_{w/2}, y_{w/2}, t_p, B) + T_n \times F_n(x_{w/2}, y_{w/2}, t_p, B) \tag{6}$$

2.2.2. Meteorological Data and Preprocessing

The daily mean temperature and daily precipitation of 28 meteorological stations located within and around the source regions of the Yangtze and Yellow Rivers were obtained from the China Meteorological Data Network (https://data.cma.cn/, accessed on 1 January 2023). First, the mean annual temperature and annual precipitation were computed site by site for each year from 1982 to 2020. Then, these two climatic factors were spatialized with a spatial resolution of 250 m by using the PER-Kriging interpolation method. Moreover, the PER-Kriging interpolation method not only considers the influence of the direction and distance of the observation point but also has the response mechanism of the elevation–precipitation correlation, with a good experimental correlation in the Lancang River Basin [45] (the distribution of the stations is shown in Figure 1):

$$Z_j^* = \sum_{i=1}^{n} \lambda_i (G(H_0 - h_i) + Z_i) + G(H_j - H_0) \tag{7}$$

where H_0 is the reference plane elevation, n is the number of observation points engaged in the interpolation computation, H_j is the elevation of the interpolation point j, h_i represents the elevation of the i-th observation point, Z_i refers to the observations from the i-th observation point, G represents the gradient of the precipitation variation with elevation, and λ_i is the weight of the i-th observation point.

The mean elevation of the study area was selected as the reference plane. The preprocessing of the observation point data was performed by using Excel 2016, while the Kriging interpolation and postprocessing were carried out in ArcMap 10.3.

2.2.3. Land Cover Data

Land cover data were obtained from the Resource and Environment Science and Data Center (https://www.resdc.cn/, accessed on 1 January 2023). The spatial resolution of the data is 30 m × 30 m. Considering the construction of ecological protection projects in the study region and the introduction of policies to protect the area, we has collected data every five years since 2000 to determine the land cover at interval times [46].

2.2.4. Topographic and Geomorphological Data

For this study, we utilized the Digital Elevation Model (DEM) obtained from NASA (https://www.earthdata.nasa.gov/, accessed on 1 January 2023). The spatial resolution is 30 m, the data type is GEOTIFF, and the coverage is global. The topographic relief, slope, and slope aspect are calculated based on the DEM; the altitude is categorized into middle altitude (1000–3500 m), high altitude (3500–5000 m), and highest altitude (>5000 m); the topographic relief is categorized into a plain (<30 m), platform hill (<200 m), low-relief mountain (200–500 m), middle-relief mountain (500–1000 m), and high-relief mountain (1000–2500 m) [47]; the aspect is classified as plain (0°), a shady aspect (0°–45°/315°–360°), a semishady aspect (45°–135°), a sunny aspect (135°–225°), and a semisunny aspect (225°–315°); and regarding the slope, 0°–5°, 5°–8°, 8°–15°, 15°–25°, 25°–35°, and >35° is classified as a gentle slope, more moderate slope, moderate slope, steep slope, steeper slope, and steepest slope [48].

2.3. Methodology

Figure 2 shows the research flowchart of this study. Initially, this study analyzes land transfer matrix changes from 1980 to 2020 in the source regions of the Yangtze and Yellow Rivers. Then, it discusses regional landscape pattern trends by using landscape indices. Furthermore, spatiotemporal vegetation cover evolution, represented by the NDVI, is examined over 40 years. Finally, statistical analysis determines land cover trends across topographic factors, and a correlation analysis quantifies the vegetation–climate relationship.

2.3.1. Land Transfer Matrix

The land transfer matrix can demonstrate the evolutionary trend in the land cover type of a specified region, and by establishing the matrix relationship between the initial and final type of various land cover types in the region, it can show the direction of the evolution of various land cover types and the area of change:

$$S_{ij} = \begin{bmatrix} S_{11} & S_{12} & \cdots & S_{1n} \\ S_{21} & S_{22} & & S_{2n} \\ & \vdots & \vdots & \vdots \\ S_{n1} & S_{n2} & \cdots & S_{nn} \end{bmatrix} \tag{8}$$

where S_{ij} indicates the area of the land-type change; n represents the number of land cover types; and i and j represent the LUCC types at the beginning and end of the study period, respectively [49].
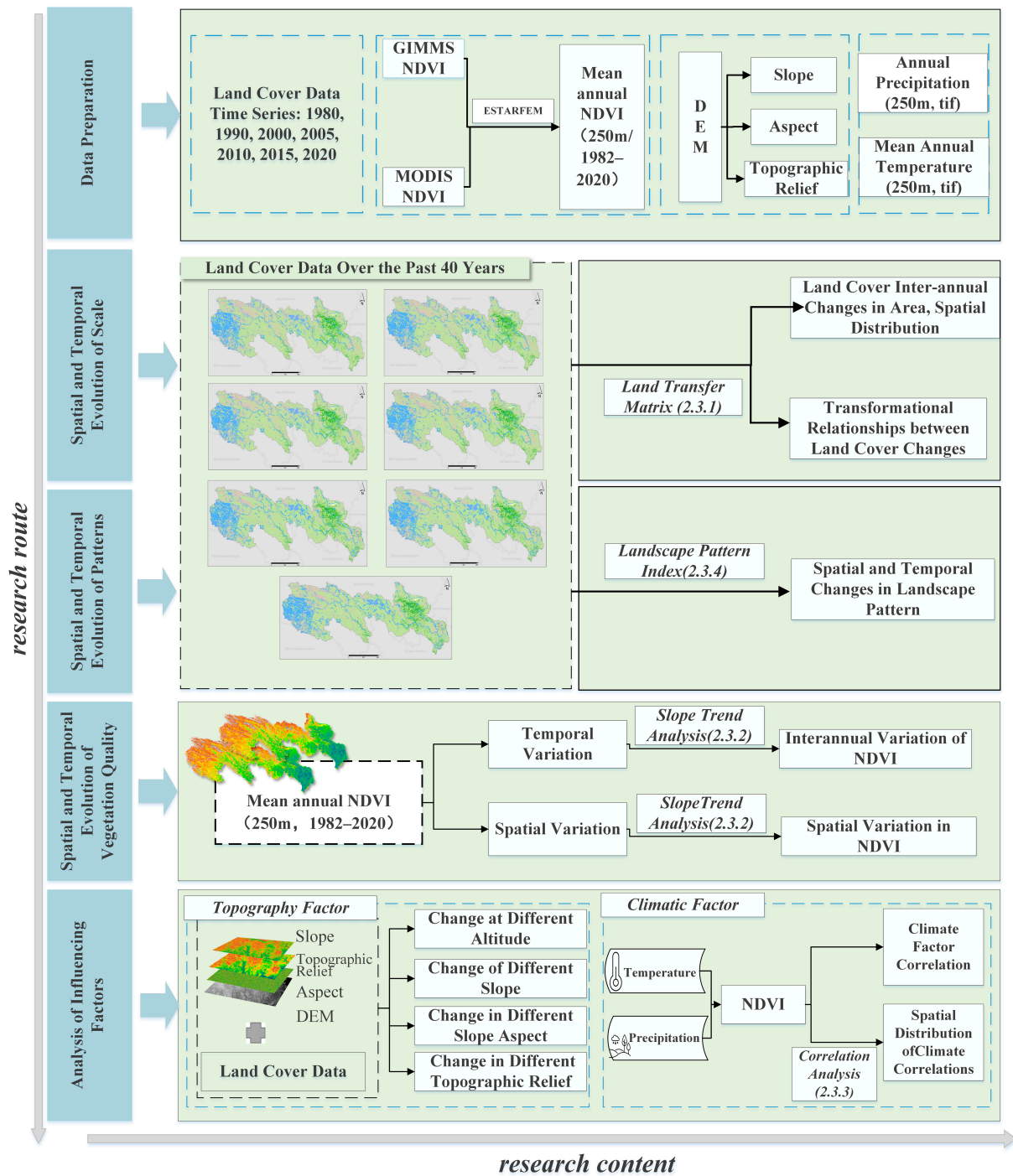
Figure 2. The research flowchart of this study.

2.3.2. Slope Trend Analysis

In order to show the spatial dynamic changes in the NDVI, a slope trend analysis was used to illustrate the pixel-wise spatial distribution of the annual NDVI variations in the study area. After calculating the NDVI values on a pixel-by-pixel basis, when *slope* > 0, the NDVI shows an increasing trend, and when *slope* < 0, the NDVI shows a decreasing trend [48]. The significance of the changes was determined by using an F-test to calculate the corresponding *p*-value [50,51]. Pixels were grouped into six categories based on the significance level exhibited by the trend: an extremely significant decline ($p \leq 0.01$), significant decrease ($0.01 < p \leq 0.05$), nonsignificant decrease ($p > 0.05$), nonsignificant

increase ($p > 0.05$), significant increase ($0.01 < p \leq 0.05$), and extremely significantly increase ($p \leq 0.01$).

The calculation formula was as follows:

$$slope = \frac{n \times \sum_{i=1}^{n}(i \times NDVI_i) - \sum_{i=1}^{n} i \sum_{i=1}^{n} NDVI_i}{n \times \sum_{i=1}^{n} i^2 - (\sum_{i=1}^{n} i)^2} \tag{9}$$

where *slope* is the linear regressing line slope, n is the number of years, and $NDVI_i$ represents the NDVI time series.

2.3.3. Correlation Analysis

The Pearson correlation coefficient (Pearson's correlation) should be used to measure the degree of linear association between two sets of continuous variables [28]:

$$r_{xy} = \frac{\sum_{i=1}^{n}(x_i - \overline{x})(y_i - \overline{y})}{\sqrt{\sum_{i=1}^{n}(x_i - \overline{x})^2 (y_i - \overline{y})^2}} \tag{10}$$

where r_{xy} is the Pearson correlation coefficient of the variables x and y; n is the number of observations; x_i, y_i are the variables x and y of the year i, respectively; and $\overline{x}$ and $\overline{y}$ are mean x and y values, respectively. In general, $r_{xy} > 0$ indicates that the two variables are positively correlated; the opposite indicates that the two variables are negatively correlated. After r_{xy} takes absolute values, 0–0.09 shows that there is no correlation, 0.1–0.3 shows a weak correlation, 0.3–0.5 shows a moderate correlation, and 0.5–1.0 shows a strong correlation [52,53].

2.3.4. Landscape Pattern Index

Land cover change is the primary determinant and direct driving force of landscape spatial patterns, and the landscape pattern index can explain the spatial structural characteristics and spatial dynamic changes in the ecological environment in the study area [54,55]. In this paper, we selected eight indicators to analyze the impact of land cover change on landscape patterns in the study area (Table 2), which was implemented by Fragstats 4.2 [56].

**Table 2.** Calculation method of landscape pattern index.

Index (Units)	Meaning	Calculation Method
Number of patches (NP)	Characterization of the landscape types in the study area and the interannual changes in the composition of different land cover types	$NP = N_i$
Landscape Division Index (LPI, %)		$LPI = \frac{M_{ax}(a_{ij})}{A}(100)$
Contagion Index (CONTAG, %)	Characterization of the association between dominant landscape types	$CONTAG = \left[1 + \frac{\sum_{i=1}^{m}\sum_{k=1}^{n}\left[(P_i(\frac{g_{ik}}{\sum_{k=1}^{m} g_{ik}})) \bullet \left[\ln(P_i)(\frac{g_{ik}}{\sum_{k=1}^{m} g_{ik}})\right]\right]}{2\ln(m)}\right](100)$
Edge density (ED, m/ha)	Characterization of landscape fragmentation degree	$ED = \frac{E}{A}(10,000)$
Mean patch size (AREA_MN, ha)		$\text{AREA\_MN} = \frac{A}{N_i}$
Aggregation Index (AI, %)		$AI = (\frac{g_{ii}}{max.g_{ii}})(100)$
Shannon's Evenness Index (SHEI)	Characterization of landscape diversity in the region in different periods	$SHDI = -\sum_{i=1}^{m}(P_i \cdot \ln P_i)$
Shannon's Diversity Index (SHDI)		$SHEI = \frac{-\sum_{i=1}^{m}(P_i \cdot \ln P_i)}{\ln m}$

Note: a_{ij} is area (m^2) of patch ij; $i = 1 \ldots m$ patch types (classes); $j = 1 \ldots n$ patches; $k = 1 \ldots k$ patches; a_{ij} = area (m^2) of patch ij; P_{ij} is perimeter (m) of patch ij; g_{ik} is number of adjacencies (joins) between pixels of patch types (classes) i and k (or i) based on the double-count method; m is number of patch types (classes) present in the landscape, including the landscape border if present; E is total length (m) of edge in landscape; A is total landscape area (m^2); and P_i is proportion of the landscape occupied by patch type (class) i.

3. Results

3.1. Temporal–Spatial Evolution Characteristics of Scale

Over the past 40 years, 8.96% of the total area of the SRYYRs has undergone LUCCs (Figure 3a). The water, grassland, and forest areas increased by 5.92%, 6.37%, and 3.95%, respectively. The plowland, industrial, and mining land increased by 42.75%, and unutilized land, such as sand, decreased by 24.49% (Figure 3b–d). This indicates that vegetation cover trends are increasing, areas of human activities and areas of water area coverage are extending, and land sanding is reducing. Changes are undeniable at the junction of two subsource regions and the southeast side of the source region of the Yellow River (Figure 4).
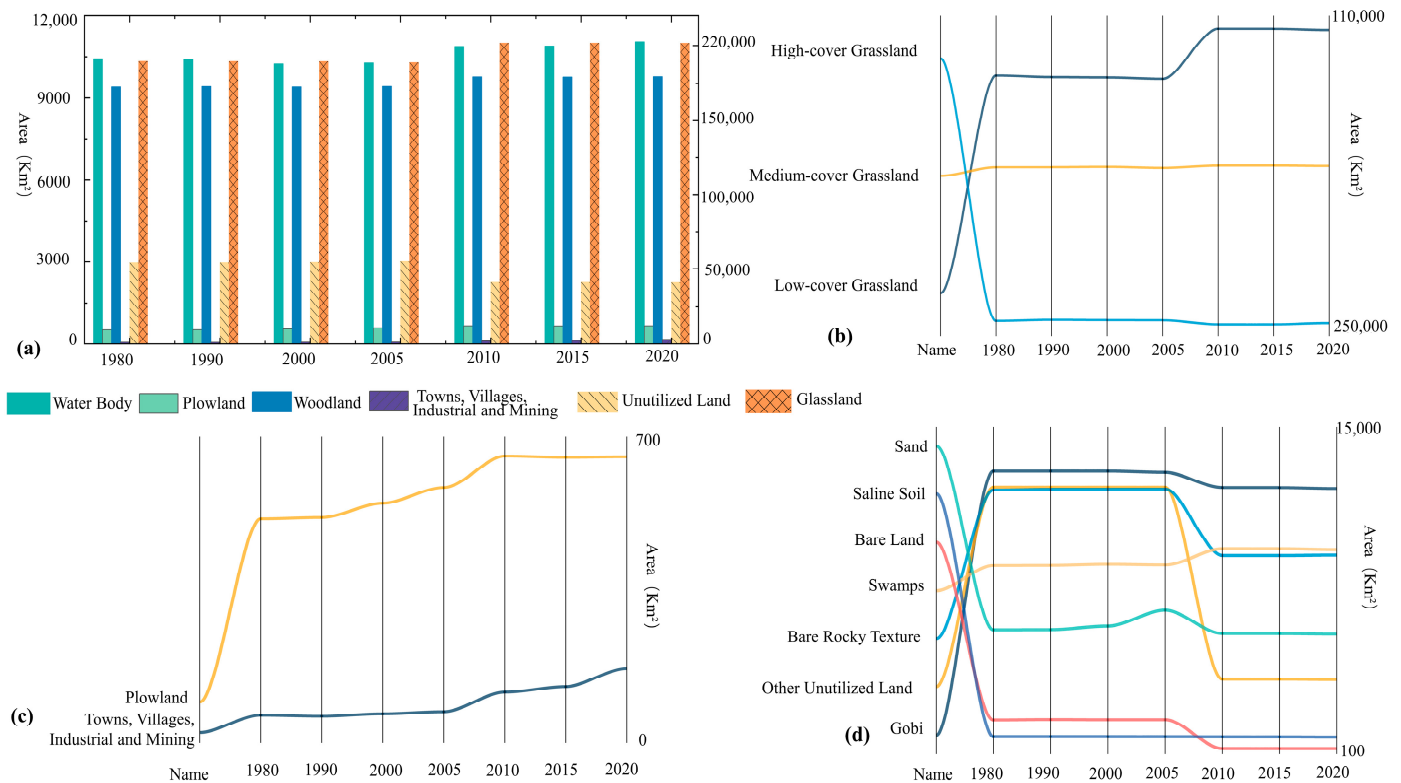
Figure 3. Interannual LUCCs in the SRYYRs from 1980 to 2020. (**a**) Land cover type trends in the SRYYRs. The left Y-axis indicates the area of the water body, plowland, woodland, towns, villages, and industrial and mining land. The right Y-axis indicates the area of grassland and unutilized land. (**b**) Grassland cover degree trends. (**c**) Trends in the area of plowland, towns, villages, and industrial and mining land. (**d**) Trends in different unutilized land types. The Y-axis in figure (**b**–**d**) is the corresponding meaning of the line.

From the spatial distribution in 2020 and the proportional area of each land cover type, it is evident that the cultivated land, towns and villages, and industrial and mining land are primarily concentrated in the source region of the Yellow River. Notably, this region exhibits a substantial moderate and high cover of grassland, constituting approximately 51.06% of the total area, while the woodland accounts for 7.36%. Conversely, the source region of the Yangtze River has lower grassland coverage, with low-coverage grassland occupying 50.27% of the area. Furthermore, the proportion of Gobi, bare rocky land, and other unutilized land in the source region of the Yangtze River is notably higher than the source region of the Yellow River, indicating a relatively severe degree of land desertification (Figure 5).
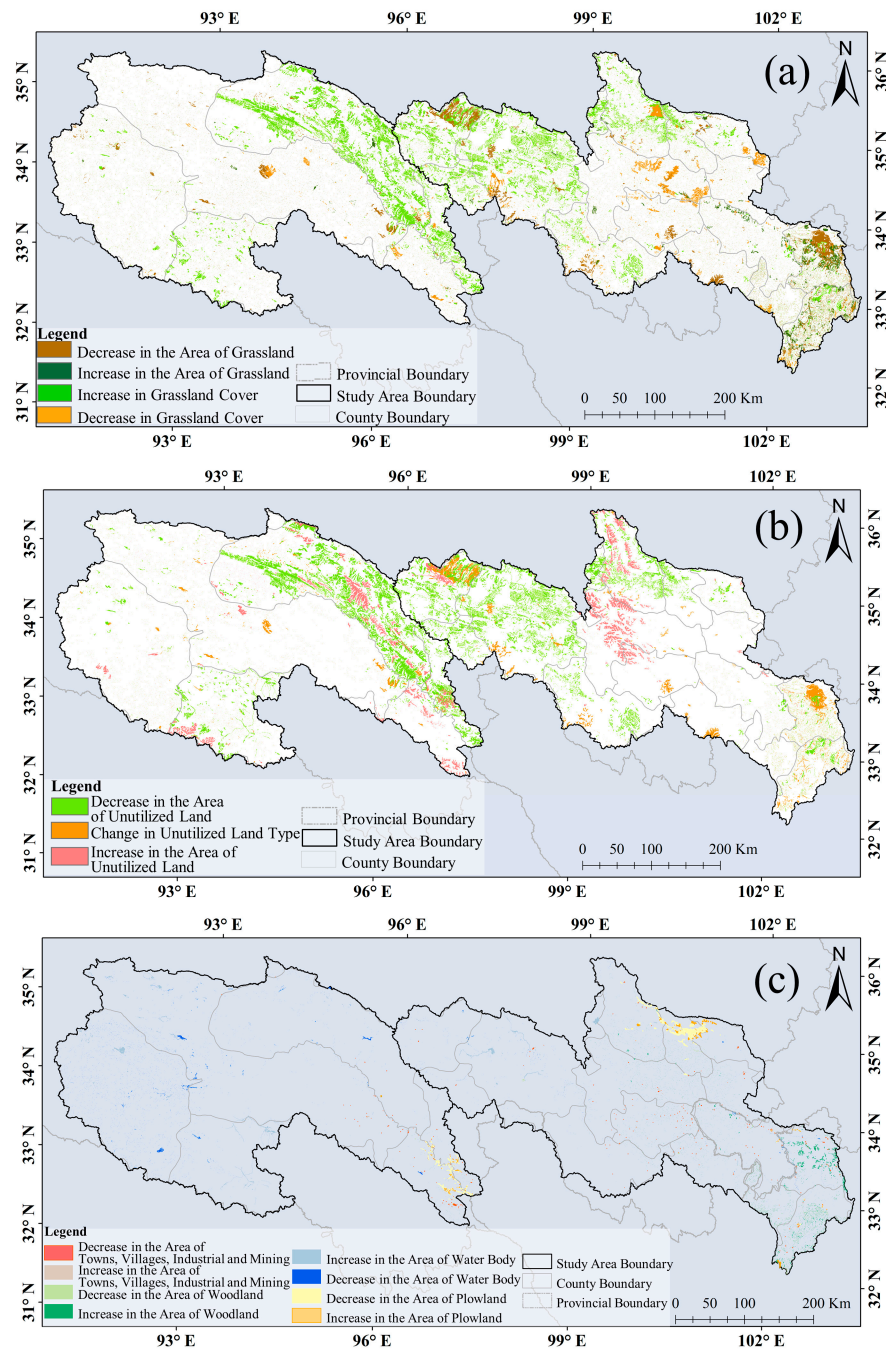
Figure 4. Map of changes in cover by land cover type from 1980 to 2020. (**a**) Spatial distribution of the location of changes in grasslands over the last 40 years. (**b**) Spatial distribution of the location of changes in unutilized land over the last 40 years. (**c**) Spatial distribution of the location of changes in water bodies, woodland, plowland, towns, villages, and industrial and mining land over the past 40 years.

The concurrent increase in vegetation cover area and degradation is observed in the source regions of both the Yangtze and Yellow Rivers, with the area of increase exceeding that of the degraded area, as depicted in Figure 4a. Specifically, the grassland area expansion is concentrated in the source region of the Yangtze River, exhibiting a growth rate 2.82% higher than that in the source region of the Yellow River. Conversely, 79.36% of grassland degradation takes place in the source region of the Yangtze River, which primarily affects high-cover grassland, particularly in the northwest vicinity of Zaling Lake, Qumalai County, and the southeast area of Zoige County (Figures 4a,b and 5). Additionally, the reduction in

the woodland area is primarily centered in the SRYYRs, with a 1.68% decrease compared to 1980. This reduction is attributed to the conversion of bush forest land and sparse forest land into medium-cover and low-cover grassland. Conversely, in the Yellow River source region, this transformation increased the woodland area. Furthermore, the degradation of permanent glacial snow is predominantly observed in the Yellow River source region, with a notable decrease of 21.39% compared to 1980, as illustrated in Figure 4c.
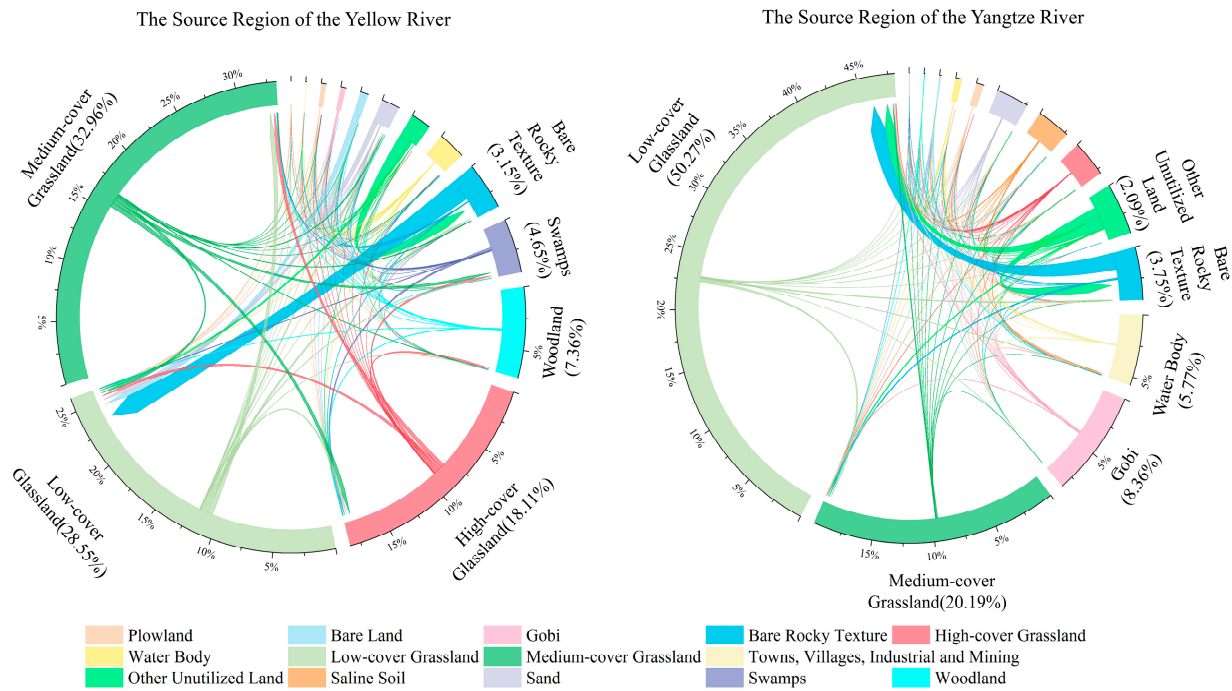
Figure 5. Land transfer matrix for the SRYYRs (pre: 1980; end: 2020). The outer circle represents the proportional area of different land cover types in 2020. The inner arrow indicates the direction of the transition of land cover type; percentage of conversion corresponds to the labeled percentage.

The crucial type of LUCC is the mutual transformation between unutilized land and grassland in the SRYYRs (Figure 5), and the transformation of grasslands into swamps is the primary type of grassland degradation in the SRYYRs. In nearly 40 years, 70.70% of the unutilized land in the study regions was transformed into grassland, and 1.28% of the grassland showed an increase in coverage (Figure 4a), particularly in the Qumalai, Chengduo, and Maduo counties at the border of the SRYYRs. All the grassland coverage in the source region of the Yangtze River showed an increasing trend. At the same time, 16.50% of the grassland was transformed into unutilized land, and 2.5%, 3.24%, and 1.09% of the high-cover, medium-cover, and low-cover grassland was transformed into swamps, respectively, where the Yellow River source region saw an increase of 15.63% in swamps. The Yangtze River source region decreased by 1.34% (Figure 5).

Drawing from Figure 6, 2005 is the key year of the ecological environment transformation in the source region of the Yangtze and Yellow Rivers. Notably, there exist distinct disparities in land cover types and rates of change between the two distinct eras. From 1980 to 2005, the region underwent significant anthropogenic influence, manifesting in the expansion of plowland, towns, villages, and industrial and mining land. Concurrently, there was a substantial reduction in the coverage of grasslands, water bodies, and swamps—critical ecosystems that regulate the climate. This decline exacerbated land desertification. From 2005 to 2020, the pace of anthropogenic activities escalated while the vegetation cover and water resources notably expanded. Furthermore, after 2010, the land cover types, excluding urban land, exhibited a tendency toward stabilization.
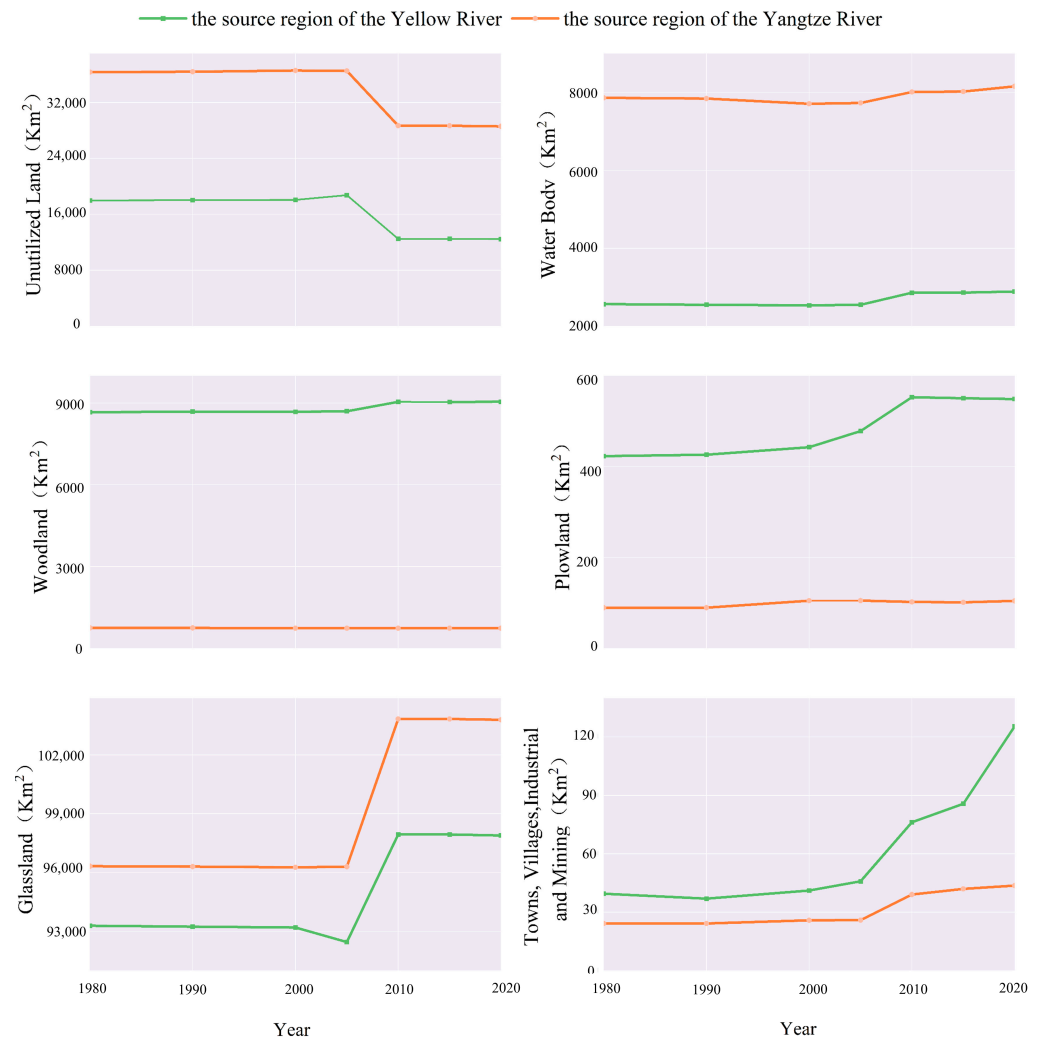
Figure 6. Interannual changes in land cover types in the SRYYRs.

3.2. Temporal–Spatial Evolution Characteristics of Pattern

In general, the LPI of the SRYYRs decreased by −6.45%, the SHEI had a relative rate of change of −6.15%, and the AI increased by 0.18% (Table 2). These observations suggest a trend toward a more homogenous landscape, with a decrease in diversity and a corresponding reduction in fragmentation. Additionally, there is enhanced connectivity between patches. The number of high-cover, middle-cover, and low-cover grassland patches showed various degrees of increase during the recent 40 years, with the most obvious being the low-cover grassland, which increased by 12.92% in 2020 compared with 1980. The degree of fragmentation of the medium-cover grassland is higher than that of the high-cover grassland and low-cover grassland. The land types with a lower degree of fragmentation in the SRYYRs are sand, other unutilized land, and high-cover grassland (Figure 7).

The long-term trends of the LPI and ED indices in the SRYYRs exhibited a pattern of "increase-decrease-increase", and the CONTAG and AREA_MN show a trend of "decrease-increase-decrease" in the long time series. Notably, the landscape indices of the SRYYRs underwent significant changes between 2000 and 2010. From 2000 to 2005, the SRYYRs showed different changes in the degree of fragmentation, landscape connectivity, and degree of clustering with that of the period. However, after 2010, the region tended toward stability in terms of landscape diversity and clustering (Table 3).
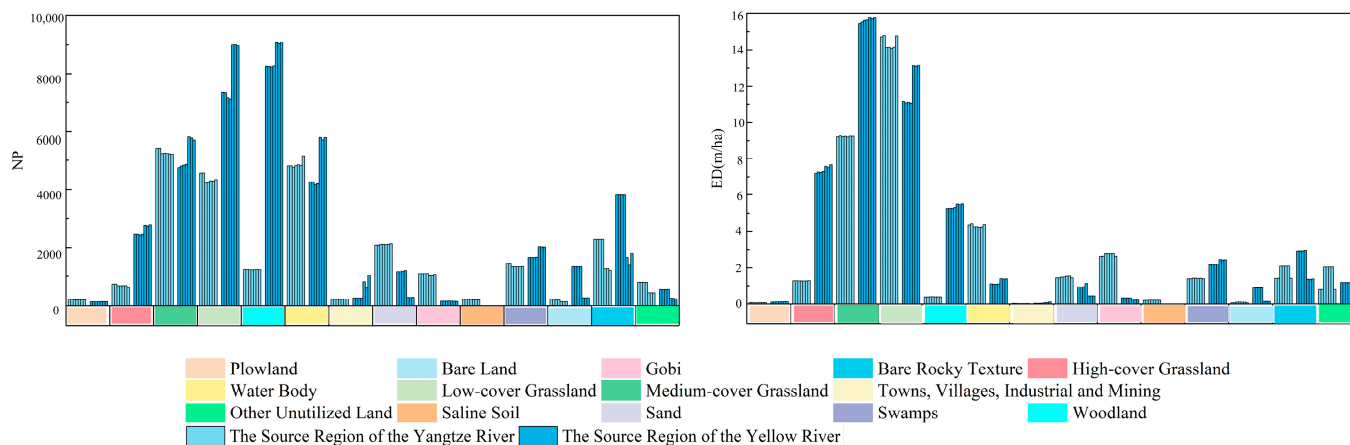
Figure 7. Interannual variations in the number of patches and edge density in SRYYRs.

Table 3. Landscape pattern index for the source region of the Yangtze and Yellow Rivers.

| Year	LPI (%)	ED (m/ha)	AREA_MN (ha)	CONTAG (%)	SHDI	SHEI	AI (%)
1980	8.23	21.88	430.05	61.19	1.95	0.62	90.14
1990	8.23	21.91	429.69	61.15	1.95	0.62	90.13
2000	8.28	21.90	437.13	61.15	1.95	0.62	90.13
2005	8.27	22.02	435.83	60.98	1.96	0.63	90.08
2010	5.57	21.46	431.76	63.51	1.83	0.58	90.33
2015	8.23	21.35	436.29	63.53	1.83	0.58	90.38
2020	5.42	21.51	426.51	63.42	1.83	0.58	90.31

Note: Landscape Division Index (LPI,%); edge density (ED, m/ha); Contagion Index (CONTAG, %); mean patch size (AREA_MN, ha); Aggregation Index (AI, %); Shannon's Evenness Index (SHEI); Shannon's Diversity Index (SHDI).

The ecological emphasis on the source regions of the Yangtze and Yellow Rivers is different, with significant differences in the landscape types between the two source areas. However, the overall trend in the changes is synchronous. In terms of the landscape diversity and uniformity, the landscape types in the source region of the Yellow River are slightly more than the source region of the Yangtze River by 0.1; the landscape uniformity is similar, so we can see that the source region of the Yellow River is enriched in terms of the land cover types, and the dominant landscapes have a high degree of connectivity. The dominant landscape types in the source region of the Yellow River are low-cover, medium-cover, and high-cover grassland, and the dominant landscape types in the source region of the Yangtze River are low-cover and medium-cover grassland and sand; it shows that the sand in the source region of the Yangtze River is more significant than that in the source region of the Yellow River. The diversity and evenness indices of both source areas have consistently changing trends. The landscape fragmentation of the source region of the Yangtze River is lower than the Yellow River source region, and the degree of clustering is higher.

3.3. Temporal–Spatial Evolution Characteristics of Vegetation Condition

Over the past 40 years, the vegetation cover in the source regions of the Yangtze and Yellow Rivers has primarily consisted of low-cover and medium-cover vegetation, exhibiting spatial heterogeneity. There is a positive trend toward improvement in the vegetation cover condition. Examining the NDVI values from 1982 to 2020, the index for the source regions of both rivers ranges between 0.1 and 0.79, with a multiyear average value maintained between 0.26 and 0.30. This indicates that the study area is mainly characterized by medium-to-low vegetation coverage. Upon analyzing the interannual changes in the mean annual NDVI, it is evident that the overall vegetation cover has exhibited a gradual upward trend (Figure 8). Observing the trend over 10 years (10a), this

upward trend is gradual, with a rate of change of 0.006/10a. The NDVI value displayed a "double peak" pattern, reaching its lowest point in 2008 and subsequently attaining the first peak in the NDVI in 2010, which represents the highest value recorded in the past 40 years. Then, it reached the peak for the second time in 2020. The rate of change in the source region of the Yellow River is 0.01/10a, and the rate of change in the source region of the Yangtze River is 0.003/10a (Figure 8).
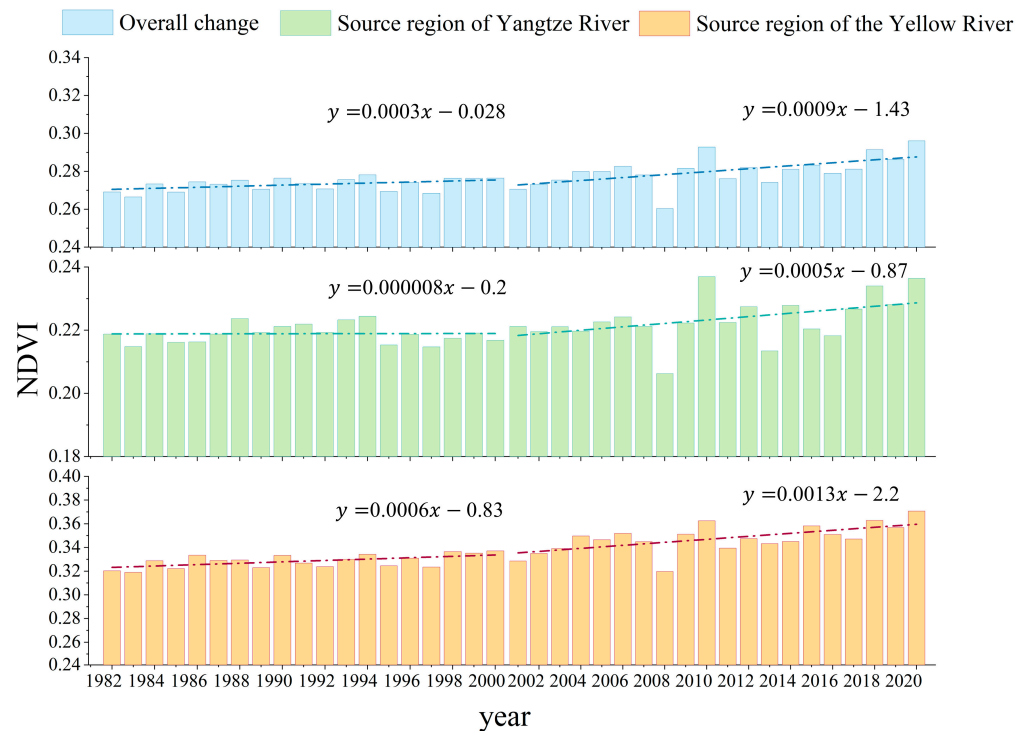

Figure 8. Interannual variation in NDVI.

Using the establishment of the Three-River Natural Reserve as a benchmark (delineating 1982–2000 as period I and 2001–2020 as period II; Figure 8), it is evident that the changes in the SRYYRs were more gradual during period I compared to the subsequent phase. Notably, the fluctuations in the mean annual NDVI values of the SRYYRs intensified from 2000 onwards, particularly between 2008 and 2010. From examining the subsource regions, it was observed that the mean annual NDVI changes in both subregions exhibited overall consistency. In the source region of the Yellow River, the mean annual NDVI change rate in period II was 2.17 times higher than that in the previous stage. This indicates a more rapid improvement in the vegetation quality in this region over this period. On the other hand, in the source region of the Yangtze River, the upward trend in the vegetation quality became evident from 2000 onwards, its mean annual NDVI remained unchanged during period I, and the growth rate during period II was lower than the rate of the Yellow River source area during the same period. This suggests that while both river source regions experienced improvement in the vegetation quality, the rate and magnitude of change differed between the two regions.

From the spatial distribution of the multiyear mean NDVI in the SRYYRs (Figure 9a), it is evident that a gradual decrease in the mean annual NDVI of vegetation occurs from the southeast towards the northwest. Specifically, the low values are mainly located in the source region of the Yangtze River and the northwest of the source region of the Yellow River. Conversely, higher NDVI values are predominantly observed in the eastern section of the Yellow River source region. When comparing the mean annual NDVI averages between the two river source regions, it is noteworthy that the Yellow River source region exhibits a mean annual NDVI of approximately 0.12 units higher than that of the Yangtze

River source region. This substantial difference indicates a significantly better vegetation cover in the Yellow River source region. Regarding the interannual trend of vegetation change, the overall quality of the SRYYRs develops a positive trend, and the quality of the vegetation in the southeast of the source region of the Yangtze decreases significantly. However, it is noteworthy that the vegetation quality in the southeastern portion of the Yangtze River source region experiences a significant decline (Figure 9b). Furthermore, the interannual trend of the NDVI change in both regions follows a similar pattern. However, the fluctuation in the vegetation cover in the source region of the Yellow River is significantly higher than in the Yangtze River source region (Figure 9b).
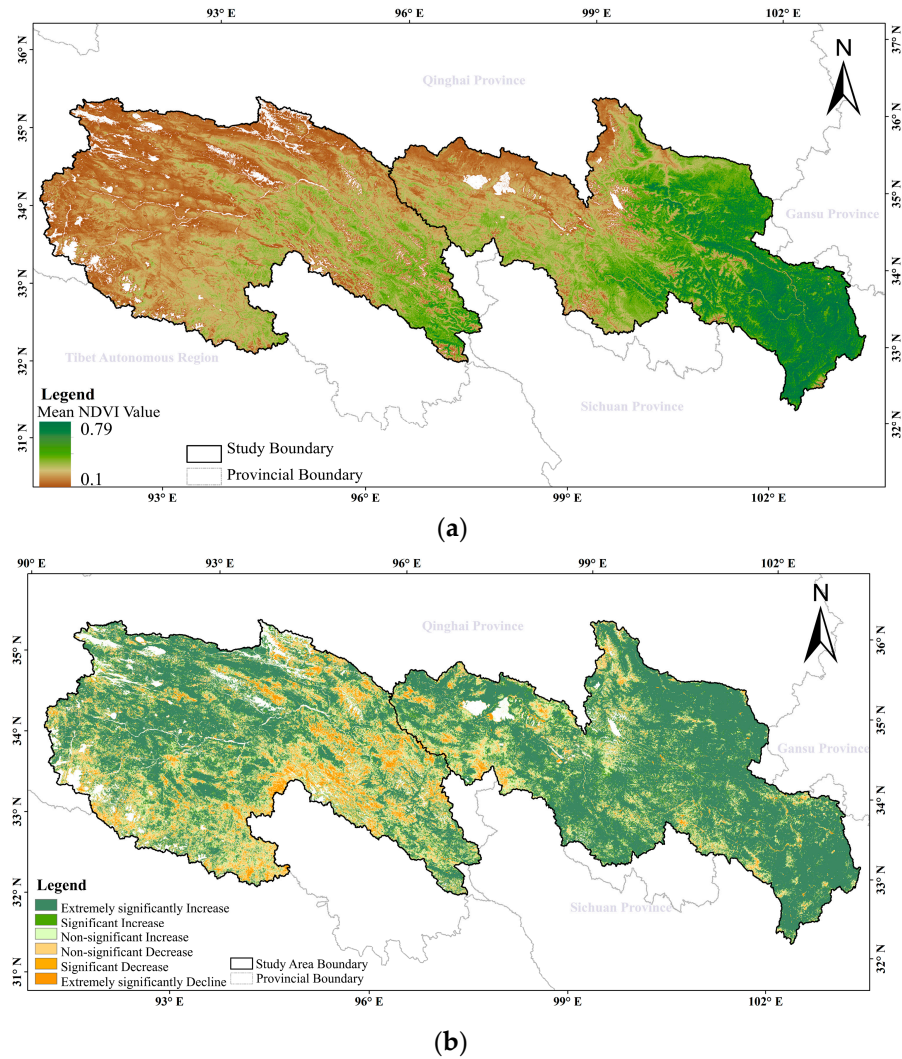
Figure 9. Spatial distribution and significance of changes in multiyear mean NDVI. (**a**) Spatial distribution of mean NDVI in the source regions of the Yangtze and Yellow Rivers in the last 40 years. (**b**) Spatial distribution of trends in mean annual NDVI values in the source regions of the Yangtze and Yellow Rivers.

3.4. Analysis of Influencing Factors

3.4.1. Analysis of the Impact of Topography

Over the past 40 years, significant changes have occurred in the SRYYRs in the middle altitude, semisunny aspect, steepest slope, and middle-relief mountain. The 2500–3500 m altitude is the interval with the most significant degree of change, with 27.54% of LUCCs in this interval, which manifests itself as the transformation of middle-cover grassland into swamps and the transformation of swamps into high-cover grassland (Figure 10a). The area of the land cover types in the middle-relief mountain changed by 57.01%, con-

centrating on the change of other unutilized land, such as alpine deserts and the tundra, into bare rocky textures and medium-cover grassland and the degradation of high-cover grassland into medium-cover grassland (Figure 10b). The area change between different slopes occurred as follows: semisunny aspect > semishady aspect > sunny aspect > shady aspect > plain (Figure 10c), which was mainly the transformation of bare rocky land into low-cover grassland and the transformation of other unutilized land into bare rocky land. In total, 66.23% of the land cover transformation of the acute steep slopes occurred in other unutilized land to low-cover grassland, and the location was concentrated on the right side of the Animachen Mountains and the southeast side of the source region of the Yangtze River, and the land cover was dominated by tundra (Figure 10d).

The two subsource regions are different in the spatial distribution of the LUCCs and the degree of change under the influence of different topographic factors. In terms of the area change, the main differences between the two subsource regions are the slope and relief intensity, with the transformation of the source region of the Yangtze River involving a high altitude, moderate slope, semisunny aspect, and low-relief mountain and the source region of the Yellow River involving the highest altitude, plains, semisunny aspect, and hill. The difference in the degree of change lies in both the altitude and slope aspects; the drastic LUCCs in the source region of the Yangtze River are the high altitude and semisunny aspect, and the source region of the Yellow River experiences the highest altitude and sunny aspect. Over the past 40 years, the sunny aspect in the source region of the Yellow River experienced 17.80% of the transformation of the land cover type; the second largest change occurred in the semisunny aspect (Figure 10).

3.4.2. Analysis of the Impact of Climate Factors

The natural transition of the land cover from nonvegetated to vegetated regions can be quantitatively assessed by using the NDVI [57]. In the source regions of the Yangtze and Yellow Rivers, grassland comprises over 70% of the total area; the area of the grassland, forest land, and cultivated land accounted for more than 80% of the total area in 2020 (Figure 5). The predominant shift in the land cover type primarily occurred between grassland and unutilized land over the past 40 years. Consequently, the NDVI is chosen as a suitable metric to quantitatively evaluate the impact of climatic factors on this land cover transition and as an indicator to describe the vegetation growth.

The climate in the source regions of the Yangtze and Yellow Rivers showed a trend of "warming-drying to warming-humidifying" in the past 40 years, with the mean annual temperature and annual precipitation decreasing gradually from southeast to northwest. In 2020, the mean annual temperature and annual precipitation increased by approximately 37.79% and 27.15%, respectively, compared to 1982 (Figure 11). In the SRYYRs over the past 40 years, the correlation between the overall mean annual NDVI and mean annual temperature was stronger than the annual precipitation, and both of them were positively correlated (Figure 12). The respective mean annual NDVI climate factor correlations of the two subsource regions obeyed the general consistency. Spatially, the regions dominated by the annual average temperature account for 76.8% of the SRYYRs, distributed in the source region of the Yellow River and the southern part of the source region of the Yangtze River; the regions dominated by annual precipitation accounted for 23.2%, located in the middle part of the source region of the Yangtze River and the northern part of the source region of the Yellow River.

From the SRYYRs as a whole, taking the year 2000 as the node (1982–2000 as period I and 2001–2020 as period II), the annual precipitation decreased at a rate of 1.35mm/year and the mean annual temperature increased at a rate of 0.048 °C/year in period I. The mean annual NDVI was moderately negatively correlated with the annual precipitation and strongly positively correlated with the mean annual temperature, with a difference of 0.24 in the absolute values of the correlation coefficients. The warming and humidification trend dominated in period II, with the trend in the increase in the annual precipitation accelerating to 4.55mm/year, the warming trend weakening to 0.03 °C/year, and the change

in the annual mean NDVI being positively correlated with both the annual precipitation and annual average temperature; additionally, the correlation was weakened compared with that in period I (Figure 13).
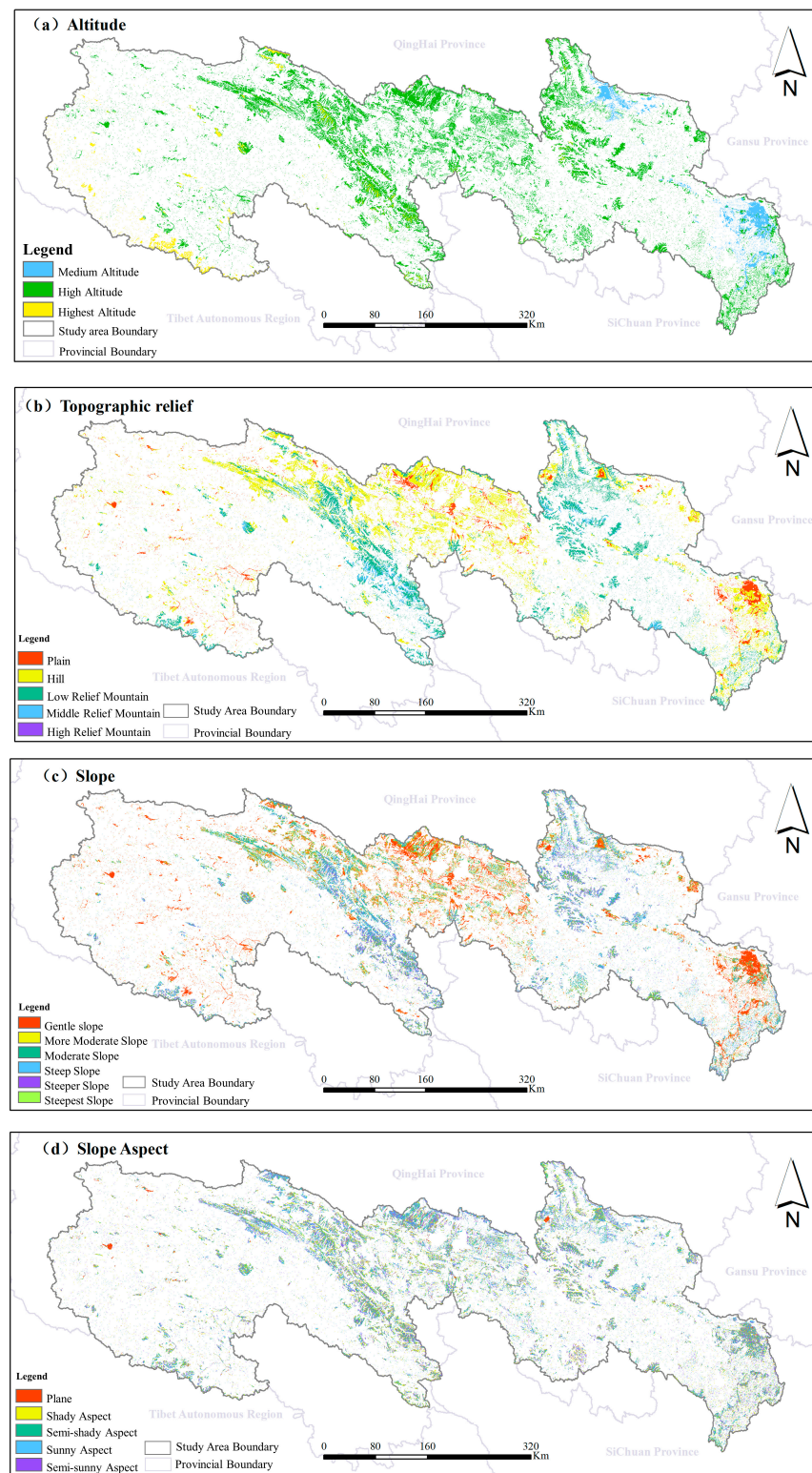

Figure 10. Spatial distribution of LUCCs due to topographic factors. (**a**) Spatial distribution of LUCC in altitude. (**b**) Spatial distribution of LUCC in topographic relief. (**c**) Spatial distribution of LUCC in slope. (**d**) Spatial distribution of LUCC in slope aspect.
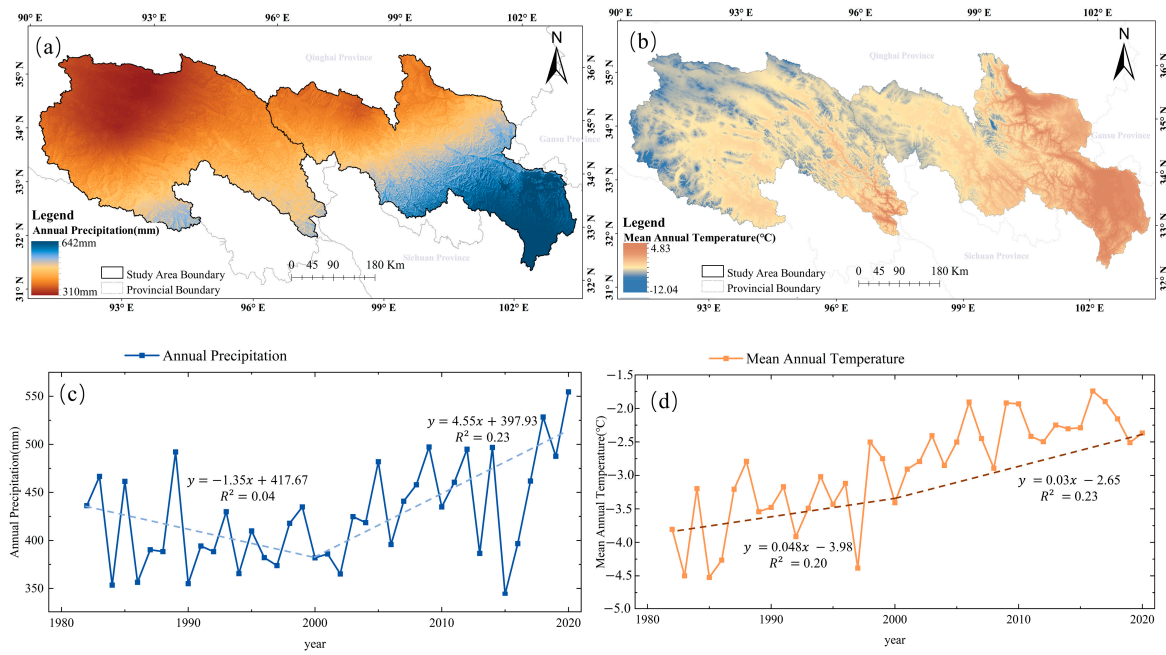
Figure 11. Spatial patterns and temporal trends in annual mean temperature and annual precipitation from 1982 to 2020. (**a**) Spatial distribution of annual precipitation; (**b**) Spatial distribution of mean annual temperature; (**c**) Trends of annual precipitation over the past 40 years; (**d**) Trend of annual mean temperature over the past 40 years.
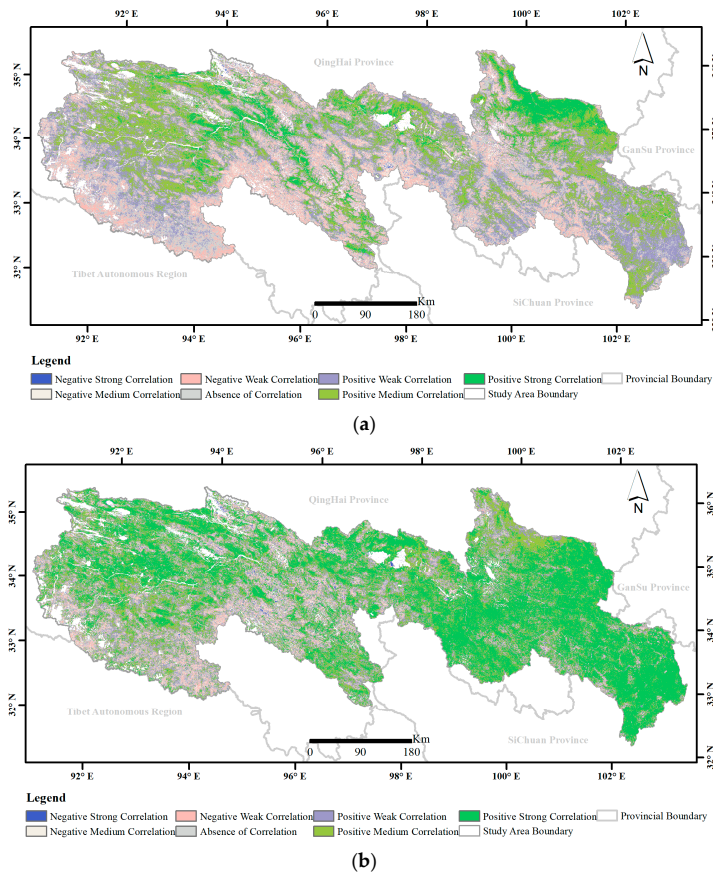
Figure 12. Spatial distribution of the correlation between mean annual NDVI, annual precipitation, and mean annual temperature. (**a**) Correlation between mean annual NDVI and annual precipitation. (**b**) Correlation between mean annual NDVI and mean annual temperature.
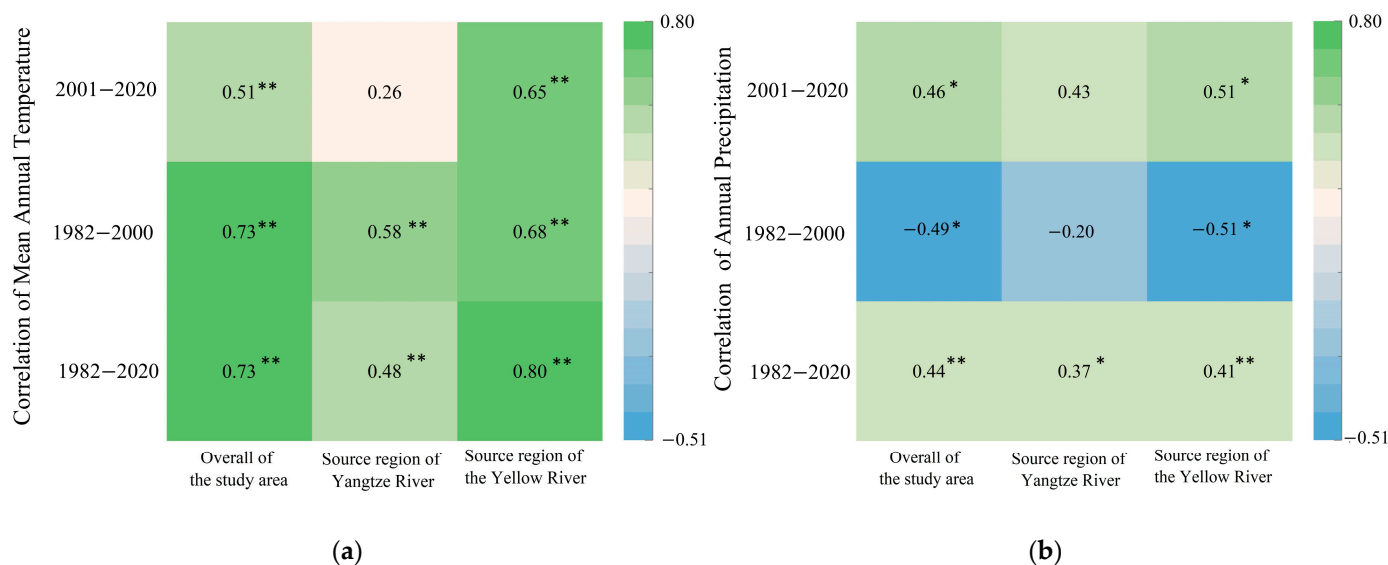
Figure 13. Mean annual NDVI correlation with annual precipitation and mean annual temperature. (**a**) Mean annual NDVI correlation with mean annual temperature; (**b**) mean annual NDVI correlation with annual precipitation (* indicates significance at the $p < 0.05$ level and ** indicates highly significant at the $p < 0.01$ level).

The correlation between the mean annual NDVI and climatic factors exhibits spatial variations across the two subregions. Both the Yellow River and Yangtze River source regions demonstrated a robust positive link in their mean annual temperature over the past 40 years. However, a notable shift occurred in the Yangtze River source region around the year 2000. The relationship between the mean annual NDVI and annual precipitation transitioned from a weak negative correlation to a moderate positive one. Concurrently, the correlation between the mean annual temperature and annual precipitation weakened from a strong positive association. In contrast, the mean annual NDVI in the Yellow River source region remains primarily influenced by the mean annual air temperature, albeit with a tendency for the correlation to weaken (Figure 13).

4. Discussion

4.1. Analysis of the Impact of Topography

Topography and inherent landform attributes play a pivotal role in shaping the distribution of vegetation communities by inducing microclimatic variations that alter their spatial patterns. Previous research has focused on the effects of altitude and slope on the spatial distribution of vegetation [26,58–61]. This study delves deeper into the degree of land cover change (LUCC) across various topography and geomorphology factors. Our findings reveal that, in the context of land cover evolution, the source regions of the Yangtze and Yellow Rivers exhibit a gradual weakening trend with increasing altitude. On the other hand, the increase in slope presents a trend of weakening and then enhancement, presenting a trend of strengthening and then weakening with increasing topographic relief (Figure 14). Notably, the stability of the land cover is more pronounced on shady and semishady slopes compared to sunny slopes. Beyond topography and landforms, LUCC is influenced by surface conditions and human activities, highlighting the complexity of the land cover dynamics.

Geomorphology is the dominant factor and fundamental element affecting the land cover structure. The middle altitude of the SRYYRs is relatively flat; human activities are concentrated and frequent, while the vegetation cover is high and varied [62,63]. Also, the hydrological cycle and ecological development in this zone are accelerated. In addition, the growth stability of low-cover grassland, which accounts for a more significant proportion in this area, is inherently poor. This area is dominated by grass-felt soil and cold calcium soil

with weak soil bioaccumulation, which has weak biological accumulation and low organic matter content at the surface, leading to a lack of soil nutrients. Furthermore, natural disasters such as mudslides have increased natural precipitation loss in areas with steep slopes, promoting LUCCs [14,64,65]. The slope aspect is an essential factor affecting vegetation cover in the tundra, and long sunshine hours and intense evapotranspiration on sunny and semisunny aspects reduce the soil moisture content and enhance the mutual transformation between grassland and unutilized land. Furthermore, it promotes the transformation of land cover types on different slope aspects. In contrast, evapotranspiration on shady slopes is relatively less, and the stability of the vegetation is more vital [66].
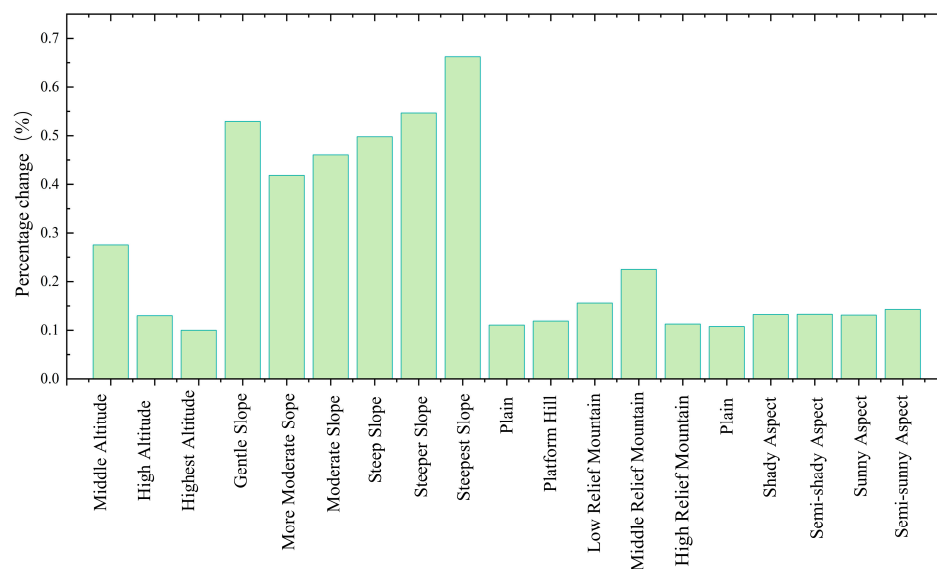
**Figure 14.** Proportion of area change by landform type.

4.2. Analysis of the Impact of Climatic Factors

This research result of the climate factor correlations in the SRYYRs is consistent with the results of historical studies [67,68]. By time period and by region of the climate factor correlation, the climatic factors that influence vegetation growth in the Yangtze River source area have undergone significant changes over the past 40 years. Geographically, the source region of the Yangtze River is an alpine region with slow vegetation growth and a short growth period. Additionally, this region showed a warm drying from 1982 to 2000, while the mean annual NDVI change increased slowly, which shows that annual precipitation did not play a prominent role in promoting vegetation growth. Since 2000, the region has witnessed a shift toward a warmer and wetter climate, characterized by augmented annual precipitation and a strengthened correlation with concurrent NDVI variations (Figure 15). It can be seen that the annual precipitation has been a key climatic factor but not a single influencing factor for the vegetation cover changes in the source region of the Yangtze River in the past 20 years.

Since 2000, the rising temperature has triggered the melting of glacial snow and permafrost, expansion of lakes, decline in surface water levels, and an upsurge in groundwater storage in the source region of the Yangtze River [69,70], which led to enhanced water resource recharge and thereby diminished the reliance of the vegetation cover on precipitation in the source region of the Yangtze River. Additionally, the implementation of safeguarding measures within the Three Rivers National Nature Reserve has resulted in the improvement in the ecological milieu in the Yangtze River's source region [26], mitigating the sole impact of augmented annual precipitation on the vegetation cover.

Vegetation is the comprehensive embodiment of ecological environmental change, driven by human activities and climate change. Climate change and ecological restoration have cooperative interactions, driving significant improvements in the vegetation cover,

carbon sequestration capacity (serving as a carbon sink), and runoff area in the region. However, the concurrent changes in the precipitation patterns and temperature introduce new risks and challenges to the region's sustainable development. Specifically, increased precipitation intensifies soil erosion and rainfall erosion, threatening the stability of recently restored ecosystems. Additionally, the rise in temperature accelerates glacier melting and permafrost degradation, altering the region's hydrological cycle and carbon cycling and potentially undermining long-term ecological gains [68,70,71].
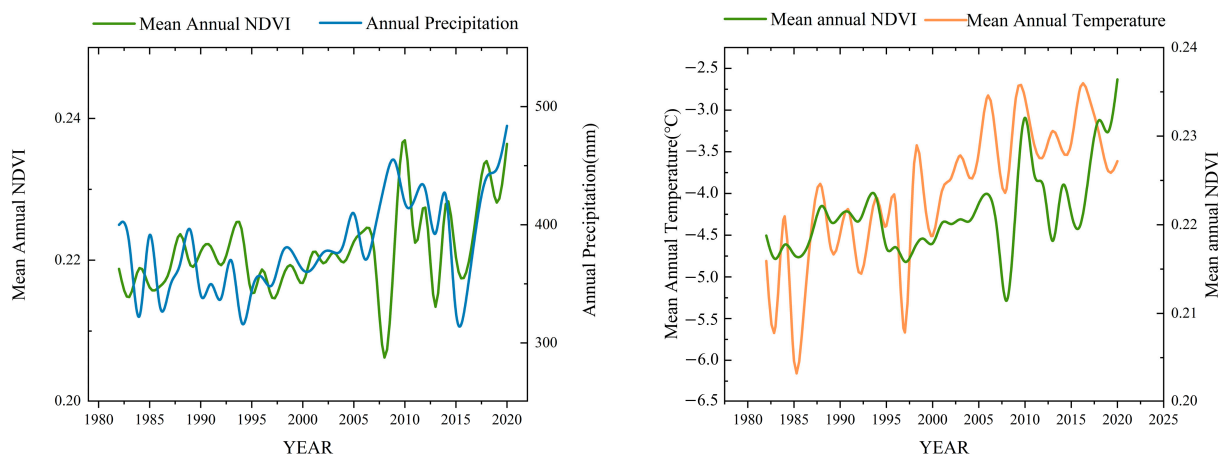
Figure 15. Relationship between mean annual temperature (**Right**), annual precipitation (**Left**), and mean annual NDVI in the source region of the Yangtze River.

The data show that the rate of change in the land cover and the change in the mean annual NDVI after 2000 are higher relative to the previous period. The area of vegetative cover has expanded, and the area of unutilized land, including sand and gravel land, has decreased. The most significant alterations occurred between 2005 and 2010. The observed shifts can partly be attributed to environmental perturbations induced by climatic factors and partly to the salutary effects of national ecological preservation efforts and ecological engineering endeavors [32,71]. Ecological relocation, the establishment of nature reserves (the source of the Yangtze River and the Yellow River, Lancang River), and the restoration of pastureland to grassland have been implemented as part of ecological restoration efforts. These measures, in conjunction with climate variability, have facilitated the ecological recovery of the region, leading to a more resilient and sustainable ecosystem [72]. For instance, mitigating the grazing intensity is pivotal for the restoration of grasslands. Following the implementation of the grazing reversal policy, the data reveal that the average livestock population within the Sanjiangyuan Reserve between 2003 and 2012 was reduced by 21.3% compared to the period from 1988 to 2002. Consequently, the grazing pressure decreased by a significant margin of 36.1%, which is positive progress toward grassland rehabilitation [73]. Climate change, human activities, and the water cycle interact and depend on each other to influence changes in surface processes and promote the improvement in the ecological environment in the region.

5. Conclusions

This study delves into the evolution of land cover; vegetation conditions; and the impact of topographical, geomorphological, and climatic factors in the source regions of the Yangtze and Yellow Rivers over the past four decades. Through rigorous analysis, the following conclusions are drawn:

(1) The source regions of the Yangtze and Yellow Rivers exhibit a discernible trend toward expanding vegetated areas, concurrent with an increase in human activity zones and an expansion of water area coverage. Areas of land degradation and

desertification have shown a decrease. The growth in vegetation cover is synchronized with degradation patterns.

(2) The overall landscape fragmentation of the source regions of the Yangtze and Yellow Rivers has decreased, while landscape diversity and uniformity have diminished. However, there is an increase in clustering, with prominent dominant landscape types emerging.

(3) The mean annual Normalized Difference Vegetation Index (NDVI) in the source regions of the Yangtze and Yellow Rivers has exhibited an upward trend. Specifically, the rate of change from 2000 to 2020 is three times that observed from 1982 to 2000. Furthermore, the annual average NDVI in the source region of the Yellow River is higher compared to that of the Yangtze River.

(4) The source regions of the Yangtze and Yellow Rivers are influenced by topography and geomorphology factors, leading to varying degrees of land cover change. Regions characterized by midaltitude, semisunny slopes, the steepest slope, and middle-relief mountains exhibit more significant changes. Furthermore, a strong correlation is observed between the annual average NDVI and annual temperature in these source regions compared to annual precipitation. Meanwhile, implementing ecological restoration measures has fostered ecological recovery in the source area.

References

1. Wang, G.; Wang, Y.; Li, Y.; Cheng, H. Influences of alpine ecosystem responses to climatic change on soil properties on the Qinghai–Tibet Plateau, China. *CATENA* **2007**, *70*, 506–514. [CrossRef]
2. Luo, D.; Jin, H.; Wu, Q.; Bense, V.F.; He, R.; Ma, Q.; Gao, S.; Jin, X.; Lü, L. Thermal regime of warm-dry permafrost in relation to ground surface temperature in the Source Areas of the Yangtze and Yellow rivers on the Qinghai-Tibet Plateau, SW China. *Sci. Total Environ.* **2018**, *618*, 1033–1045. [CrossRef] [PubMed]
3. Gao, Q.; Guo, Y.; Xu, H.; Ganjurjav, H.; Li, Y.; Wan, Y.; Qin, X.; Ma, X.; Liu, S. Climate change and its impacts on vegetation distribution and net primary productivity of the alpine ecosystem in the Qinghai-Tibetan Plateau. *Sci. Total Environ.* **2016**, *554–555*, 34–41. [CrossRef] [PubMed]
4. Hao, S.; Zhu, F.; Cui, Y. Land use and land cover change detection and spatial distribution on the Tibetan Plateau. *Sci Rep.* **2021**, *11*, 7531. [CrossRef] [PubMed]
5. Yao, T.D.; Thompson, L.; Yang, W.; Yu, W.S.; Gao, Y.; Guo, X.J.; Yang, X.X.; Duan, K.Q.; Zhao, H.B.; Xu, B.Q.; et al. Different glacier status with atmospheric circulations in Tibetan Plateau and surroundings. *Nat. Clim. Change* **2012**, *2*, 663–667. [CrossRef]
6. Xu, W.; Ma, L.; Ma, M.; Zhang, H.; Yuan, W. Spatial–Temporal Variability of Snow Cover and Depth in the Qinghai–Tibetan Plateau. *J. Clim.* **2017**, *30*, 1521–1533. [CrossRef]
7. Xue, Z.; Lyu, X.; Chen, Z.; Zhang, Z.; Jiang, M.; Zhang, K.; Lyu, Y. Spatial and Temporal Changes of Wetlands on the Qinghai-Tibetan Plateau from the 1970s to 2010s. *Chin. Geogr. Sci.* **2018**, *28*, 935–945. [CrossRef]
8. Li, Y.; Hou, Z.; Zhang, L.; Qu, Y.; Zhou, G.; Lin, J.; Li, J.; Huang, K. Long-term spatio-temporal changes of wetlands in Tibetan Plateau and their response to climate change. *Int. J. Appl. Earth Obs. Geoinf.* **2023**, *121*, 103351. [CrossRef]
9. Wang, L. Characterization of water use efficiency changes in Tibetan Plateau grasslands based on eco-geographic zoning. *Environ. Sci. Pollut. Res.* **2022**, *30*, 26998–27012. [CrossRef]
10. Jiang, W.; Lü, Y.; Liu, Y.; Gao, W. Ecosystem service value of the Qinghai-Tibet Plateau significantly increased during 25 years. *Ecosyst. Serv.* **2020**, *44*, 101146. [CrossRef]
11. Li, Y.; Gong, J.; Zhang, Y.; Gao, B. NDVI-Based Greening of Alpine Steppe and Its Relationships with Climatic Change and Grazing Intensity in the Southwestern Tibetan Plateau. *Land* **2022**, *11*, 975. [CrossRef]

12. Yang, Y.; Wu, Q.; Jin, H.; Wang, Q.; Huang, Y.; Luo, D.; Gao, S.; Jin, X. Delineating the hydrological processes and hydraulic connectivities under permafrost degradation on Northeastern Qinghai-Tibet Plateau, China. *J. Hydrol.* **2019**, *569*, 359–372. [CrossRef]

13. Wei, Y.; Lu, H.; Wang, J.; Wang, X.; Sun, J. Dual Influence of Climate Change and Anthropogenic Activities on the Spatiotemporal Vegetation Dynamics Over the Qinghai-Tibetan Plateau From 1981 to 2015. *Earth's Future* **2022**, *10*, e2021EF002566. [CrossRef]

14. Pan, Y.; Wang, Y.; Zheng, S.; Huete, A.R.; Shen, M.; Zhang, X.; Huang, J.; He, G.; Yu, L.; Xu, X.; et al. Characteristics of Greening along Altitudinal Gradients on the Qinghai–Tibet Plateau Based on Time-Series Landsat Images. *Remote Sens.* **2022**, *14*, 2408. [CrossRef]

15. Zhang, F.; Hu, X.; Zhang, J.; Li, C.; Zhang, Y.; Li, X. Change in Alpine Grassland NPP in Response to Climate Variation and Human Activities in the Yellow River Source Zone from 2000 to 2020. *Sustainability* **2022**, *14*, 8790. [CrossRef]

16. Liu, G.; Shao, Q.; Fan, J.; Ning, J.; Huang, H.; Liu, S.; Zhang, X.; Niu, L.; Liu, J. Spatio-Temporal Changes, Trade-Offs and Synergies of Major Ecosystem Services in the Three-River Headwaters Region from 2000 to 2019. *Remote Sens.* **2022**, *14*, 5349. [CrossRef]

17. Li, Z.; Lyu, S.; Chen, H.; Ao, Y.; Zhao, L.; Wang, S.; Zhang, S.; Meng, X. Changes in climate and snow cover and their synergistic influence on spring runoff in the source region of the Yellow River. *Sci. Total Environ.* **2021**, *799*, 149503. [CrossRef]

18. Li, X.; Zhang, Y.; Yan, H.; Salahou, M.K. Watershed-level spatial pattern of degraded alpine meadow and its key influencing factors in the Yellow River Source Zone of West China. *Ecol. Indic.* **2023**, *146*, 109865. [CrossRef]

19. Qin, Y.; Yang, D.; Gao, B.; Wang, T.; Chen, J.; Chen, Y.; Wang, Y.; Zheng, G. Impacts of climate warming on the frozen ground and eco-hydrology in the Yellow River source region, China. *Sci. Total Environ.* **2017**, *605–606*, 830–841. [CrossRef]

20. Shi, R.; Yang, H.; Yang, D. Spatiotemporal variations in frozen ground and their impacts on hydrological components in the source region of the Yangtze River. *J. Hydrol.* **2020**, *590*, 125237. [CrossRef]

21. Liu, L.; Jiang, L.; Wang, H.; Ding, X.; Xu, H. Estimation of glacier mass loss and its contribution to river runoff in the source region of the Yangtze River during 2000–2018. *J. Hydrol.* **2020**, *589*, 125207. [CrossRef]

22. Yi, W.; Feng, Y.; Liang, S.; Kuang, X.; Yan, D.; Wan, L. Increasing annual streamflow and groundwater storage in response to climate warming in the Yangtze River source region. *Environ. Res. Lett.* **2021**, *16*, 084011. [CrossRef]

23. Cui, X.; Graf, H.-F. Recent land cover changes on the Tibetan Plateau: A review. *Clim. Change* **2009**, *94*, 47–61. [CrossRef]

24. Na, L.; Wang, G.; Liu, G.; Lin, Y.; Sun, X. The ecological implications of land use change in the Source Regions of the Yangtze and Yellow Rivers, China. *Reg. Environ. Change* **2013**, *13*, 1099–1108. [CrossRef]

25. Ren, X.; Dong, Z.; Hu, G.; Zhang, D.; Li, Q. A GIS-Based Assessment of Vulnerability to Aeolian Desertification in the Source Areas of the Yangtze and Yellow Rivers. *Remote Sens.* **2016**, *8*, 626. [CrossRef]

26. Liu, L.; Cao, W.; Shao, Q.; Huang, L.; He, T. Characteristics of Land Use/Cover and Macroscopic Ecological Changes in the Headwaters of the Yangtze River and of the Yellow River over the Past 30 Years. *Sustainability* **2016**, *8*, 237. [CrossRef]

27. Li, F.-F.; Lu, H.-L.; Wang, G.-Q.; Yao, Z.-Y.; Li, Q.; Qiu, J. Zoning of precipitation regimes on the Qinghai–Tibet Plateau and its surrounding areas responded by the vegetation distribution. *Sci. Total Environ.* **2022**, *838*, 155844. [CrossRef]

28. Gao, S.; Dong, G.; Jiang, X.; Nie, T.; Guo, X. Analysis of factors influencing spatiotemporal differentiation of the NDVI in the upper and middle reaches of the Yellow River from 2000 to 2020. *Front. Environ. Sci.* **2023**, *10*, 1072430. [CrossRef]

29. Gao, S.; Dong, G.; Jiang, X.; Nie, T.; Yin, H.; Guo, X. Quantification of Natural and Anthropogenic Driving Forces of Vegetation Changes in the Three-River Headwater Region during 1982–2015 Based on Geographical Detector Model. *Remote Sens.* **2021**, *13*, 4175. [CrossRef]

30. Liu, X.; Zhu, X.; Zhu, W.; Pan, Y.; Zhang, C.; Zhang, D. Changes in Spring Phenology in the Three-Rivers Headwater Region from 1999 to 2013. *Remote Sens.* **2014**, *6*, 9130–9144. [CrossRef]

31. Zhai, X.; Liang, X.; Yan, C.; Xing, X.; Jia, H.; Wei, X.; Feng, K. Vegetation Dynamic Changes and Their Response to Ecological Engineering in the Sanjiangyuan Region of China. *Remote Sens.* **2020**, *12*, 4035. [CrossRef]

32. Guo, B.; Wang, J.; Mantravadi, V.S.; Zhang, L.; Liu, G. Effect of climate and ecological restoration on vegetation changes in the "Three-River Headwaters" region based on remote sensing technology. *Environ. Sci. Pollut. Res.* **2022**, *29*, 16436–16448. [CrossRef]

33. Deng, X.; Hu, S.; Zhan, C. Attribution of vegetation coverage change to climate change and human activities based on the geographic detectors in the Yellow River Basin, China. *Environ. Sci. Pollut. Res.* **2022**, *29*, 44693–44708. [CrossRef]

34. Pan, T.; Wu, S.; Liu, Y. Relative Contributions of Land Use and Climate Change to Water Supply Variations over Yellow River Source Area in Tibetan Plateau during the Past Three Decades. *PLoS ONE* **2015**, *10*, e0123793. [CrossRef]

35. Lu, Z.; Song, Q.; Zhao, J. Evolution of Landscape Ecological Risk and Identification of Critical Areas in the Yellow River Source Area Based on LUCC. *Sustainability* **2023**, *15*, 9749. [CrossRef]

36. Yang, Z.; Gao, J.; Zhou, C.; Shi, P.; Zhao, L.; Shen, W.; Ouyang, H. Spatio-temporal changes of NDVI and its relation with climatic variables in the source regions of the Yangtze and Yellow rivers. *J. Geogr. Sci.* **2011**, *21*, 979–993. [CrossRef]

37. Shang, Z.H.; Ma, Y.S.; Long, R.J.; Ding, L.M. Effect of fencing, artificial seeding and abandonment on vegetation composition and dynamics of 'black soil land' in the headwaters of the Yangtze and the Yellow Rivers of the Qinghai-Tibetan Plateau. *Land Degrad. Dev.* **2008**, *19*, 554–563. [CrossRef]

38. Pang, G.; Wang, X.; Yang, M. Using the NDVI to identify variations in, and responses of, vegetation to climate change on the Tibetan Plateau from 1982 to 2012. *Quat. Int.* **2017**, *444*, 87–96. [CrossRef]

39. Mao, X.; Ren, H.-L.; Liu, G.; Su, B.; Sang, Y. Influence of the Indian Summer Monsoon on Inter-Annual Variability of the Tibetan-Plateau NDVI in Its Main Growing Season. *Remote Sens.* **2023**, *15*, 3612. [CrossRef]

40. Du, J.; He, P.; Fang, S.; Liu, W.; Yuan, X.; Yin, J. Autumn NDVI contributes more and more to vegetation improvement in the growing season across the Tibetan Plateau. *Int. J. Digit. Earth* **2017**, *10*, 1098–1117. [CrossRef]

41. Wang, G.; Ding, Y.; Wang, J.; Liu, S. Land ecological changes and evolutional patterns in the source regions of the Yangtze and Yellow Rivers in recent 15 years. *Acta Geogr. Sin.* **2004**, *59*, 163–173.

42. Dai, X.; Fan, W.; Shan, Y.; Gao, Y.; Liu, C.; Nie, R.; Zhang, D.; Li, W.; Zhang, L.; Sun, X.; et al. LAI-Based Phenological Changes and Climate Sensitivity Analysis in the Three-River Headwaters Region. *Remote Sens.* **2022**, *14*, 3748. [CrossRef]

43. Fan, X.; Gao, P.; Tian, B.; Wu, C.; Mu, X. Spatio-Temporal Patterns of NDVI and Its Influencing Factors Based on the ESTARFM in the Loess Plateau of China. *Remote Sens.* **2023**, *15*, 2553. [CrossRef]

44. Zhu, X.; Chen, J.; Gao, F.; Chen, X.; Masek, J.G. An enhanced spatial and temporal adaptive reflectance fusion model for complex heterogeneous regions. *Remote Sens. Environ.* **2010**, *114*, 2610–2623. [CrossRef]

45. Wang, S.; Yan, D.; Qin, T.; Liu, R.H. Spatial interpolation of precipitation using the PER-Kriging method. *Adv. Water Sci.* **2011**, *22*, 756–763.

46. Qinghai Three Rivers Nature Reserve Ecological Protection and Construction Master Plan. Available online: https://www.ndrc. gov.cn/fzggw/jgsj/njs/sjdt/201404/t20140411_1194723.html (accessed on 1 January 2023).

47. Zhou, C.; Cheng, W.; Qian, J.; Li, B.; Zhang, B. Research on the Classification System of Digital Land Geomorphology of 1:1,000,000 in China. *Geo.-Inf. Sci.* **2010**, *11*, 707–724. [CrossRef]

48. Feng, J.; Dong, B.; Qin, T.; Liu, S.; Zhang, J.; Gong, X. Temporal and Spatial Variation Characteristics of NDVI and Its Relationship with Environmental Factors in Huangshui River Basin from 2000 to 2018. *Pol. J. Environ. Stud.* **2021**, *30*, 3043–3063. [CrossRef]

49. Lu, Z.; Song, Q.; Zhao, J.; Ding, Y. Changes in Ecological Land Patterns and Divergence Trends in Yellow River Source Area from 2005 to 2020. *Bull. Soil. Water Conserv.* **2022**, *42*, 277–284. [CrossRef]

50. Chen, S.-T.; Guo, B.; Yang, F.; Han, B.-M.; Fan, Y.-W.; Yang, X.; He, T.-L.; Liu, Y.; Yang, W.-N. Spatial and temporal patterns of NPP and its response to climate change in the Qinghai-Tibet Plateau from 2000 to 2015. *J. Nat. Resour.* **2020**, *35*, 2511. [CrossRef]

51. Liu, X.; Zhang, J.; Zhu, X.; Pan, Y.; Liu, Y.; Zhang, D.; Lin, Z. Spatiotemporal changes in vegetation coverage and its driving factors in the Three-River Headwaters Region during 2000–2011. *J. Geogr. Sci.* **2014**, *24*, 288–302. [CrossRef]

52. Muller, K. Statistical Power Analysis for the Behavioral Sciences. *Technometrics* **1989**, *31*, 499–500. [CrossRef]

53. Ren, Y.; Liu, J.; Liu, S.; Wang, Z.; Liu, T.; Shalamzari, M.J. Effects of Climate Change on Vegetation Growth in the Yellow River Basin from 2000 to 2019. *Remote Sens.* **2022**, *14*, 687. [CrossRef]

54. Duan, X.; Chen, Y.; Wang, L.; Zheng, G.; Liang, T. The impact of land use and land cover changes on the landscape pattern and ecosystem service value in Sanjiangyuan region of the Qinghai-Tibet Plateau. *J. Environ. Manag.* **2023**, *325*, 116539. [CrossRef]

55. Yang, H.; Zhong, X.; Deng, S.; Nie, S. Impact of LUCC on landscape pattern in the Yangtze River Basin during 2001–2019. *Ecol. Inform.* **2022**, *69*, 101631. [CrossRef]

56. Jia, Y.; Tang, L.; Xu, M.; Yang, X. Landscape pattern indices for evaluating urban spatial morphology—A case study of Chinese cities. *Ecol. Indic.* **2019**, *99*, 27–37. [CrossRef]

57. Wang, Z.; Wu, J.; Niu, B.; He, Y.; Zu, J.; Li, M.; Zhang, X. Vegetation Expansion on the Tibetan Plateau and Its Relationship with Climate Change. *Remote Sens.* **2020**, *12*, 4150. [CrossRef]

58. Zhang, Q.-P.; Fang, R.-Y.; Deng, C.-Y.; Zhao, H.-J.; Shen, M.-H.; Wang, Q. Slope aspect effects on plant community characteristics and soil properties of alpine meadows on Eastern Qinghai-Tibetan plateau. *Ecol. Indic.* **2022**, *143*, 109400. [CrossRef]

59. Zhang, X.; Wang, J.; Gao, Y.; Wang, L. Variations and controlling factors of vegetation dynamics on the Qingzang Plateau of China over the recent 20 years. *Geogr. Sustain.* **2021**, *2*, 74–85. [CrossRef]

60. Chen, D.; Li, Q.; Liu, Z.; He, F.; Chen, X.; Xu, S.; Zhao, X.; Zhao, L. Variations of Forage Yield and Nutrients with Altitude Gradients and Their Influencing Factors in Alpine Meadow of Sanjiangyuan, China. *J. Soil Sci. Plant. Nutr.* **2020**, *20*, 2164–2174. [CrossRef]

61. Liu, N.; Yang, Y.; Yao, L.; Yue, X. A Regionalized Study on the Spatial-Temporal Changes of Grassland Cover in the Three-River Headwaters Region from 2000 to 2016. *Sustainability* **2018**, *10*, 3539. [CrossRef]

62. Gao, S.; Dong, G.; Jiang, X.; Nie, T.; Guo, X.; Dang, S.; Li, X.; Li, H. Analysis of vegetation coverage changes and natural driving forces of spatial distribution in the source region of the Yellow River. *Ecol. Environ. Sci.* **2022**, *31*, 429–439. [CrossRef]

63. Yang, Y.; You, Q.; Zuo, Z.; Zhang, Y.; Liu, Z.; Kang, S.; Zhai, P. Elevation dependency of temperature trend over the Qinghai-Tibetan Plateau during 1901–2015. *Atmos. Res.* **2023**, *290*, 106791. [CrossRef]

64. Guo, B.; Han, F.; Jiang, L. An Improved Dimidiated Pixel Model for Vegetation Fraction in the Yarlung Zangbo River Basin of Qinghai-Tibet Plateau. *J. Indian Soc. Remote Sens.* **2018**, *46*, 219–231. [CrossRef]

65. Qin, Q.; Chen, J.; Yang, Y.; Zhao, X.; Zhou, G.; You, H.; Han, X. Spatiotemporal variations of vegetation and its response to topography and climate in the source region of the Yellow River. *China Environ. Sci.* **2021**, *41*, 3832–3841. [CrossRef]

66. Wang, H.; Liu, D.; Lin, H.; Montenegro, A.; Zhu, X. NDVI and vegetation phenology dynamics under the influence of sunshine duration on the Tibetan plateau. *Int. J. Climatol.* **2015**, *35*, 687–698. [CrossRef]

67. Pan, T.; Zou, X.; Liu, Y.; Wu, S.; He, G. Contributions of climatic and non-climatic drivers to grassland variations on the Tibetan Plateau. *Ecol Eng.* **2017**, *108*, 307–317. [CrossRef]

68. Zhang, K.; Li, X. Responses of vegetation growth to climate change over the Tibetan Plateau from 1982 to 2018. *Environ. Res. Commun.* **2022**, *4*, 045007. [CrossRef]

69. Cao, H.; Gao, B.; Gong, T.; Wang, B. Analyzing Changes in Frozen Soil in the Source Region of the Yellow River Using the MODIS Land Surface Temperature Products. *Remote Sens.* **2021**, *13*, 180. [CrossRef]

70. Jin, X.; Jin, H.; Luo, D.; Sheng, Y.; Wu, Q.; Wu, J.; Wang, W.; Huang, S.; Li, X.; Liang, S.; et al. Impacts of Permafrost Degradation on Hydrology and Vegetation in the Source Area of the Yellow River on Northeastern Qinghai-Tibet Plateau, Southwest China. *Front. Earth Sci.* **2022**, *10*, 845824. [CrossRef]

71. Jiang, C.; Zhang, L. Ecosystem change assessment in the Three-river Headwater Region, China: Patterns, causes, and implications. *Ecol. Eng.* **2016**, *93*, 24–36. [CrossRef]

72. Shao, Q.; Cao, W.; Fan, J.; Huang, L.; Xu, X. Effects of an ecological conservation and restoration project in the Three-River Source Region, China. *J. Geogr. Sci.* **2017**, *27*, 183–204. [CrossRef]

73. Zhang, L.; Fan, J.; Zhou, D.; Zhang, H. Ecological Protection and Restoration Program Reduced Grazing Pressure in the Three-River Headwaters Region, China. *Rangel. Ecol. Manag.* **2017**, *70*, 540–548. [CrossRef]